INFLAMMATION

The heavy subunit of ferritin stimulates NLRP3 inflammasomes in hepatic stellate cells through ICAM-1 to drive hepatic inflammation

Manuel A. Fernandez-Rojo[1,2,3,4]*, Michael A. Pearen[1], Anita G. Burgess[1], Maria P. Ikonomopoulou[1,2,5,6], Diem Hoang-Le[1], Berit Genz[1], Silvia L. Saggiomo[1], Sujeevi S. K. Nawaratna[1], Maura Poli[7], Regina Reissmann[8], Geoffrey N. Gobert[1,9], Urban Deutsch[10], Britta Engelhardt[10], Andrew J. Brooks[4], Alun Jones[6], Paolo Arosio[7], Grant A. Ramm[1,2]*

Serum ferritin concentrations increase during hepatic inflammation and correlate with the severity of chronic liver disease. Here, we report a molecular mechanism whereby the heavy subunit of ferritin (FTH) contributes to hepatic inflammation. We found that FTH induced activation of the NLRP3 inflammasome and secretion of the proinflammatory cytokine interleukin-1β (IL-1β) in primary rat hepatic stellate cells (HSCs) through intercellular adhesion molecule–1 (ICAM-1). FTH–ICAM-1 stimulated the expression of *Il1b*, NLRP3 inflammasome activation, and the processing and secretion of IL-1β in a manner that depended on plasma membrane remodeling, clathrin-mediated endocytosis, and lysosomal destabilization. FTH–ICAM-1 signaling at early endosomes stimulated *Il1b* expression, implying that this endosomal signaling primed inflammasome activation in HSCs. In contrast, lysosomal destabilization was required for FTH-induced IL-1β secretion, suggesting that lysosomal damage activated inflammasomes. FTH induced IL-1β production in liver slices from wild-type mice but not in those from *Icam1*$^{-/-}$ or *Nlrp3*$^{-/-}$ mice. Thus, FTH signals through its receptor ICAM-1 on HSCs to activate the NLRP3 inflammasome. We speculate that this pathway contributes to hepatic inflammation, a key process that stimulates hepatic fibrogenesis associated with chronic liver disease.

INTRODUCTION

Iron is a vital trace element required to maintain normal cellular physiology. In mammalian cells, iron is stored within ferritin, a multiprotein complex of 24 subunits with varying tissue-specific composition of two subunit types, heavy ferritin (FTH) and light ferritin (FTL), that prevents cellular iron cytotoxicity (*1*, *2*). Ferritin is mostly found inside cells; however, during hepatic inflammation and the development of chronic liver disease (such as non-alcoholic steatohepatitis or chronic viral hepatitis B or C), excessive concentrations of circulating ferritin (hyperferritinemia) often exist, which can reflect saturated body iron stores (in hemochromatosis) (*3*) or act as an indicator of chronic liver disease severity (*3*–*6*). Previously, we have shown that extracellular FTH protein (independent of iron content) stimulates interleukin-1β (*IL1B*) expression in hepatic stellate cells (HSCs) in a manner that depends on protein kinase Cζ (PKCζ) and nuclear factor κB (NF-κB) signaling (*7*).

Because HSCs are collagen-producing myofibroblasts that are pivotally involved in driving inflammation and fibrogenesis associated with chronic liver disease, we propose that FTH acts as a signaling molecule that contributes to liver inflammation. Here, we investigated how FTH might induce proinflammatory responses in HSCs and identified intercellular adhesion molecule–1 (ICAM-1) as the FTH receptor responsible for FTH-induced IL-1β secretion in HSCs. IL-1β maturation and secretion rely on the cleavage and activation of caspase-1 coordinated by the inflammasome, a multimeric protein complex assembled in response to diverse external physiological and pathogenic stimuli (*8*, *9*). Inflammasome activation requires two signals: a priming signal and an activation signal. The priming signal induces transcriptional responses, such as receptor-mediated NF-κB–dependent increases in pro–IL-1β and the NACHT, LRR and PYD domains–containing proteins (NLRs), of which NLRP1 and NLRP3 are the most well-characterized cell sensors forming inflammasomes (*10*). The secondary signal activates NLRPs and triggers the formation of inflammasomes and the activation of caspase-1, which promotes IL-1β processing and secretion (*10*). In this context, FTH signaling appeared to induce both priming and activation of the NLRP3 inflammasome and therefore caspase-1–driven IL-1β maturation. We also provide evidence that this process is assisted by clathrin-coated pit (CCP) endocytosis, with early and late endosomes constituting a major component of the cellular platform for transduction of FTH–ICAM-1 signaling. Thus, we hypothesize that FTH acts as a damage-associated molecular pattern (DAMP) that signals through ICAM-1 to promote IL-1β secretion in HSCs.

RESULTS

FTH stimulates inflammasome activation in HSCs

FTH stimulated *IL1B* gene expression in the human HSC cell line LX-2, similarly to our previous findings in primary rat HSCs (*7*), supporting a potential pathophysiological role of FTH in human HSCs during the development of liver inflammation (fig. S1A). In primary rat HSCs, human

[1]QIMR Berghofer Medical Research Institute, Brisbane, Herston, QLD 4006, Australia. [2]School of Medicine, University of Queensland, Brisbane, Herston, QLD 4006, Australia. [3]Hepatic Regenerative Medicine Laboratory, Madrid Institute for Advanced Studies in Food, Madrid 28049, Spain. [4]University of Queensland Diamantina Institute, University of Queensland, Translational Research Institute, Brisbane, QLD 4102, Australia. [5]Translational Venomics Laboratory, Madrid Institute for Advanced Studies in Food, Madrid 28049, Spain. [6]Institute for Molecular Bioscience, University of Queensland, Brisbane, QLD 4072, Australia. [7]Department of Molecular and Translational Medicine, University of Brescia, Brescia, Italy. [8]Department for BioMedical Research (DBMR), University of Bern, Freiestrasse 1, CH-3012 Bern, Switzerland. [9]School of Biological Sciences, Queen's University Belfast, Belfast, UK. [10]Theodor Kocher Institute, University of Bern, Freiestrasse 1, CH-3012 Bern, Switzerland.
*Corresponding author. Email: grant.ramm@qimrberghofer.edu.au (G.A.R.); mafernaro@hotmail.com (M.A.F.-R.)

recombinant FTH, generated in *Escherichia coli* and depleted of potential lipopolysaccharide (LPS) contamination by endotoxin removal, stimulated the induction of NLRP3 (but not NLRP1) similarly to LPS, which we used as a positive control for inflammasome activation (Fig. 1A). Consistent with inflammasome activation, FTH induced pro–IL-1β protein, which was cleaved into the mature, bioactive form of IL-1β (Fig. 1A). Moreover, FTH induced the inflammasome-adaptor protein apoptosis–associated speck-like protein containing a caspase activation and recruitment domain (ASC) (Fig. 1, B to D). Confocal imaging showed that ASC exhibited high colocalization with IL-1β protein in FTH-treated cells (Fig. 1C). Unlike in immune cells, neither FTH- nor LPS-treated primary rat HSCs exhibited classical ASC speck formation (Fig. 1, B and C).

To validate these results, we tested commercial endotoxin-free recombinant human FTH generated in human embryonic kidney (HEK) 293 cells on primary rat HSCs. We compared the activity of this FTH preparation with commercial HEK293-derived endotoxin-free recombinant FTL because a previous study showed minor effects of FTL, relative to FTH, on specific aspects of HSC activation (*7*). HEK293-derived FTH exhibited similar induction of *IL1B* transcripts (fig. S1B) and IL-1β protein secretion (fig. S1C), coinciding with an increase in NLRP3 protein (fig. S1D). Conversely, knockdown (KD) of *Nlrp1* or *Nlrp3* in FTH-treated primary rat HSCs significantly reduced the secretion of mature, cleaved IL-1β (Fig. 1E) without significantly affecting *Il1b* transcripts (fig. S1E), underscoring the dependence of FTH

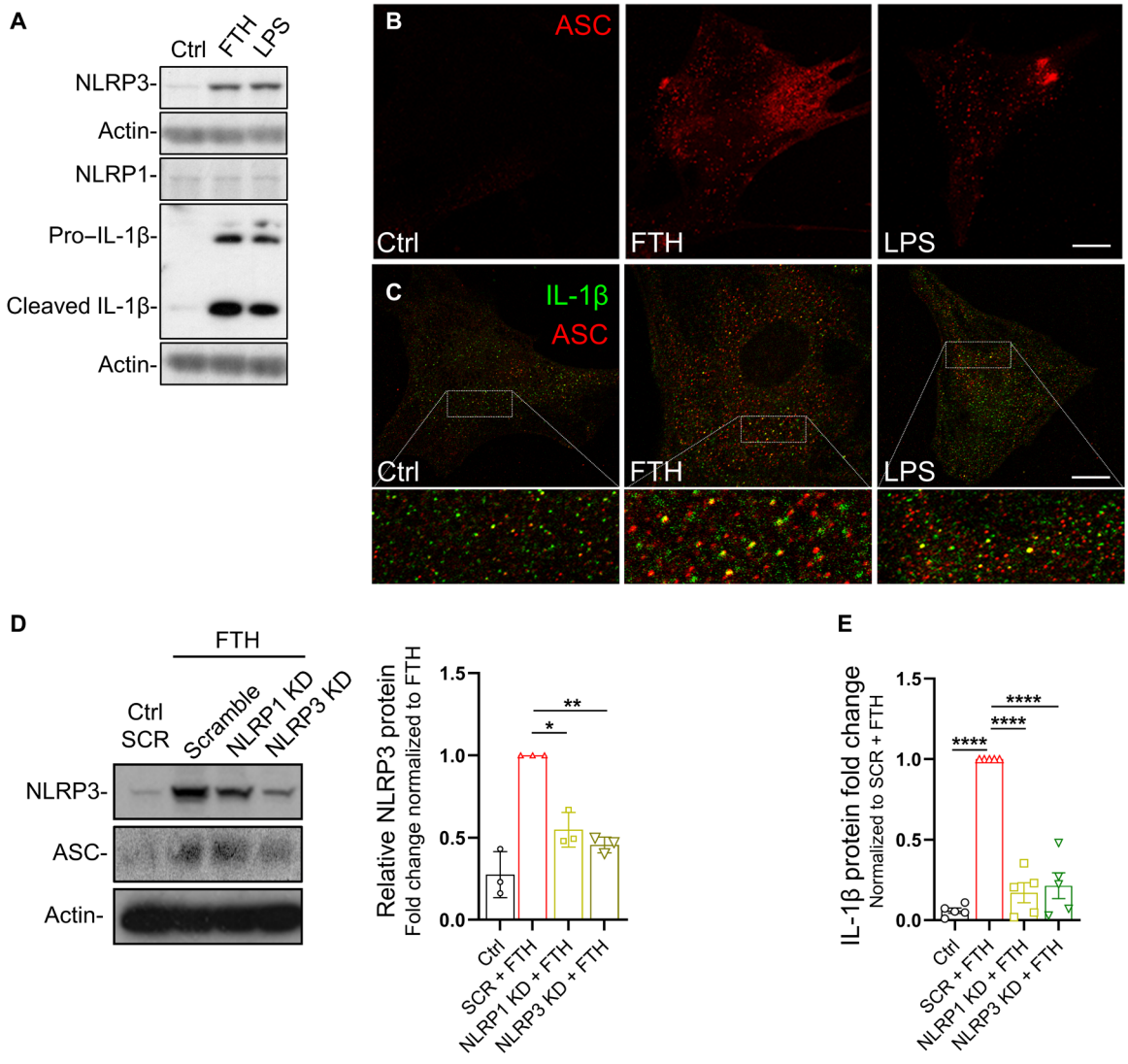

Fig. 1. FTH stimulates inflammasome activation in rat HSCs. (**A**) Representative Western blot showing NLRP1, NLRP3, and both pro- and cleaved (active) forms of IL-1β in primary rat HSCs treated with LPS or FTH for 4 hours. Blot is representative of $n = 3$ independent experiments. Actin is a loading control. (**B** and **C**) Immunofluorescence showing ASC (B) or ASC and IL-1β (C) in primary rat HSCs stimulated with FTH or LPS for 24 hours. Images are representative of $n = 3$ independent experiments. Scale bars, 20 μm. (**D**) Representative Western blot showing ASC and NLRP3 in untreated primary rat HSCs expressing a scrambled siRNA (Ctrl SCR) or in cells expressing scrambled siRNA or siRNAs for NLRP1 or NLRP3 KD and treated with FTH for 24 hours. NLRP3 protein was quantified relative to the actin loading control and normalized to the amount in the SCR-FTH group. Blot is representative of $n = 3$ independent experiments. (**E**) Quantification of IL-1β secreted into the culture medium by primary rat HSCs treated with FTH. $n = 5$ independent experiments. Results in bar graphs are presented as mean (fold change) ± SEM. Statistical analysis was performed using a repeated measures one-way ANOVA (paired) with Šídák's multiple comparisons test, where $P \leq 0.05$ was considered statistically significant. *$P \leq 0.05$, **$P \leq 0.01$, and ****$P \leq 0.001$.

signaling on the activation and assembly of the inflammasome. Although FTH had no effect on NLRP1 protein (Fig. 1A), *Nlrp1* KD partially inhibited FTH-induced NLRP3 stimulation (Fig. 1D) that, together with decreased secretion of IL-1β (Fig. 1E), suggested that NLRP1 might play a role in NLRP3-inflammasome integrity. FTL produced some induction of *Il1b* mRNA expression; however, this was significantly lower compared with FTH (fig. S1B) and did not include induction of IL-1β secretion (fig. S1C) or NLRP3 protein (fig. S1D).

ICAM-1 is the FTH receptor in HSCs

We wanted to identify the receptor to which FTH was binding in HSCs. Previous studies have shown that FTH interacts with T cell immunoglobulin and mucin domain containing-2 (TIM-2) in oligodendrocytes (*11*) and in B cells from the kidney and liver (*12*) in mice and with transferrin receptor-1 (TfR1) on human B and T cells (*13*) and erythroid cells (*14*–*17*). However, because these proteins exhibit low (micromolar) binding affinity for FTH, it is unlikely that they constitute the HSC-FTH signaling receptor, given that our previous work showed that FTH exhibits very high (nanomolar) affinity binding on primary rat HSCs (*18*). Transient inhibition of signaling by the chaperone glucose-regulated protein-78 (GRP78) using a fusion protein of epidermal growth factor and subtilase cytotoxin A (EGF-SubA) abolishes IL-1β and tumor necrosis factor (TNF) secretion in response to human serum containing ferritin in rat primary HSCs (*19*). However, no direct effect of ferritin was demonstrated in this study, and human serum contains many other potential proinflammatory mediators that may have affected the secretion of IL-1β and TNF.

To identify the FTH-signaling receptor in HSCs, we used two different and independent unbiased screening methods. First, primary rat HSCs were exposed to Alexa Fluor 488 (AF488)–labeled recombinant human FTH followed by nano–high-performance liquid chromatography tandem mass spectrometry (HPLC-MS/MS) to examine the major fluorescently labeled FTH–cross-linked protein bands in cell membrane fractions separated by electrophoresis (Fig. 2A). Among the set of proteins, we identified GRP78 in more than one band and the cell surface–bound adhesion molecule ICAM-1 (Fig. 2A), which we have previously described as an FTH-induced NF-κB–regulated gene in rat HSCs (*7*). To validate these potential receptor candidates, we used ligand-receptor glycocapture technology (DualSystems Biotech) using the cross-linking agent TriCEPS. This approach revealed ICAM-1 as the only FTH receptor candidate within the dictated robust statistical parameters where the protein enrichment factor was >4-fold and the analysis of variance (ANOVA) pairwise comparison false discovery rate–adjusted P value was $P < 0.01$ (Fig. 2B). High-molecular weight kininogen (HKa), a previously demonstrated FTH-binding protein (*20*), emerged as a second potential candidate with relevant enrichment. HKa is of interest because it binds ICAM-1 and is a known inhibitor of the ICAM-1 cell adhesion complex mediated by the integrin CD11b/CD18 (integrin $\alpha_M\beta_2$, also known as Mac-1) (*21*). However, HKa binding to FTH did not reach statistical significance. Thus, we conclude that ICAM-1 is the most likely FTH receptor candidate in primary rat HSCs. Supporting this, loss- and gain-of-function experiments showed that overexpression of green fluorescent protein–tagged human ICAM-1 (ICAM-1–GFP) in FTH-treated primary rat HSCs (fig. S2A) significantly increased (65.7 ± 0.23%) FTH-induced *Il1b* mRNA (Fig. 2C), whereas KD of ICAM-1 (ICAM1 KD) by ~75% in primary rat HSCs using a pool of three different small interfering RNAs (siRNAs) (fig. S2B) significantly decreased FTH-induced *Il1b* expression (54.18 ± 0.08% of SCR + FTH; Fig. 2D).

After the priming signal that induces *Il1b* expression, an activation signal is required for the inflammasome activation and assembly that results in the cleavage and activation of caspase-1 and caspase-1–mediated cleavage of pro–IL-1β protein into active IL-1β for secretion. As further evidence of inflammasome activation, FTH markedly increased the secretion of cleaved IL-1β into the culture medium (Fig. 1E), which correlated with an increase in both pro– and activated (cleaved) caspase-1 (p20 fragment) in primary rat HSCs (Fig. 2E and fig. S2, D and E). Furthermore, ICAM1 KD also inhibited the induction of NLRP3 protein (Fig. 2E and fig. S2C), as well as both pro– and cleaved caspase-1 (Fig. 2E and fig. S2, D and E) by FTH, and this was coupled with an almost complete inhibition of IL-1β secretion (Fig. 2F). To provide further supporting evidence for the role of ICAM-1 in FTH-induced proinflammatory signaling, we transfected immortalized human hepatocyte (IHH) cells, a human liver cell line with very low endogenous *ICAM1* expression compared with HepG2 and Hep3G cells (Fig. 2G), with an *ICAM1* expression plasmid, resulting in significantly increased expression of *ICAM-1* (Fig. 2H). Treatment of wild-type (WT) IHH cells with FTH had no effect on *IL1B* expression; however, FTH induced a marked increase in *IL1B* expression in IHH cells overexpressing ICAM-1 compared with control cells transfected with the empty plasmid (Fig. 2I).

KD of another FTH-binding protein, GRP78 (GRP78 KD; ~70% mRNA KD), in primary rat HSCs (fig. S3A) had no effect on either FTH-induced *Il1b* (fig. S3B) or *Icam1* (fig. S3C) gene expression. However, *Grp78* deficiency blunted the induction of NLRP3 (fig. S3D) and the secretion of IL-1β protein elicited by FTH (fig. S3E), suggesting that GRP78 does not affect FTH–ICAM-1–induced inflammasome priming but may play a downstream role in FTH–ICAM-1–induced inflammasome assembly and activation.

FTH induces IL-1β through ICAM-1 and the NLRP3 inflammasome in liver tissue

Next, we questioned the potential pathophysiological relevance of FTH-induced inflammation in the context of liver disease. Because we do not have an in vivo approach to mimic pathological concentrations of circulating FTH in mice, we exposed precision-cut liver tissue slices from WT mice to high (pathological) concentrations of recombinant human FTH ex vivo. Precision-cut liver slices were also treated with LPS as a positive control for *Il1b* stimulation. Under these conditions, we observed that FTH significantly stimulated *Il1b* expression in liver slices from WT mice (Fig. 3A). Using precision-cut liver slices from *Nlrp1* (*Nlrp1*$^{-/-}$) and *Nlrp3* (*Nlrp3*$^{-/-}$) knockout mice and WT control mice of the same genetic background as the knockouts, we observed that loss of *Nlrp1* or *Nlrp3* did not prevent FTH-induced increases in *Il1b* gene expression (Fig. 3, B to D). FTH induced mature IL-1β protein in liver slices from WT and *Nlrp1*$^{-/-}$ mice but not in tissue from *Nlrp3*$^{-/-}$ mice (Fig. 3E). We also examined the potential pathophysiological relevance of ICAM-1 in the stimulation and maturation of IL-1β by FTH. Consistent with the results from our experiments in primary rat HSCs, ICAM-1 deficiency also reduced FTH-induced *Il1b* gene expression in liver tissue slices from ICAM-1 knockout (*ICAM1*$^{-/-}$) mice (Fig. 3F), supporting the pathophysiological relevance of FTH–ICAM-1 interaction in the liver.

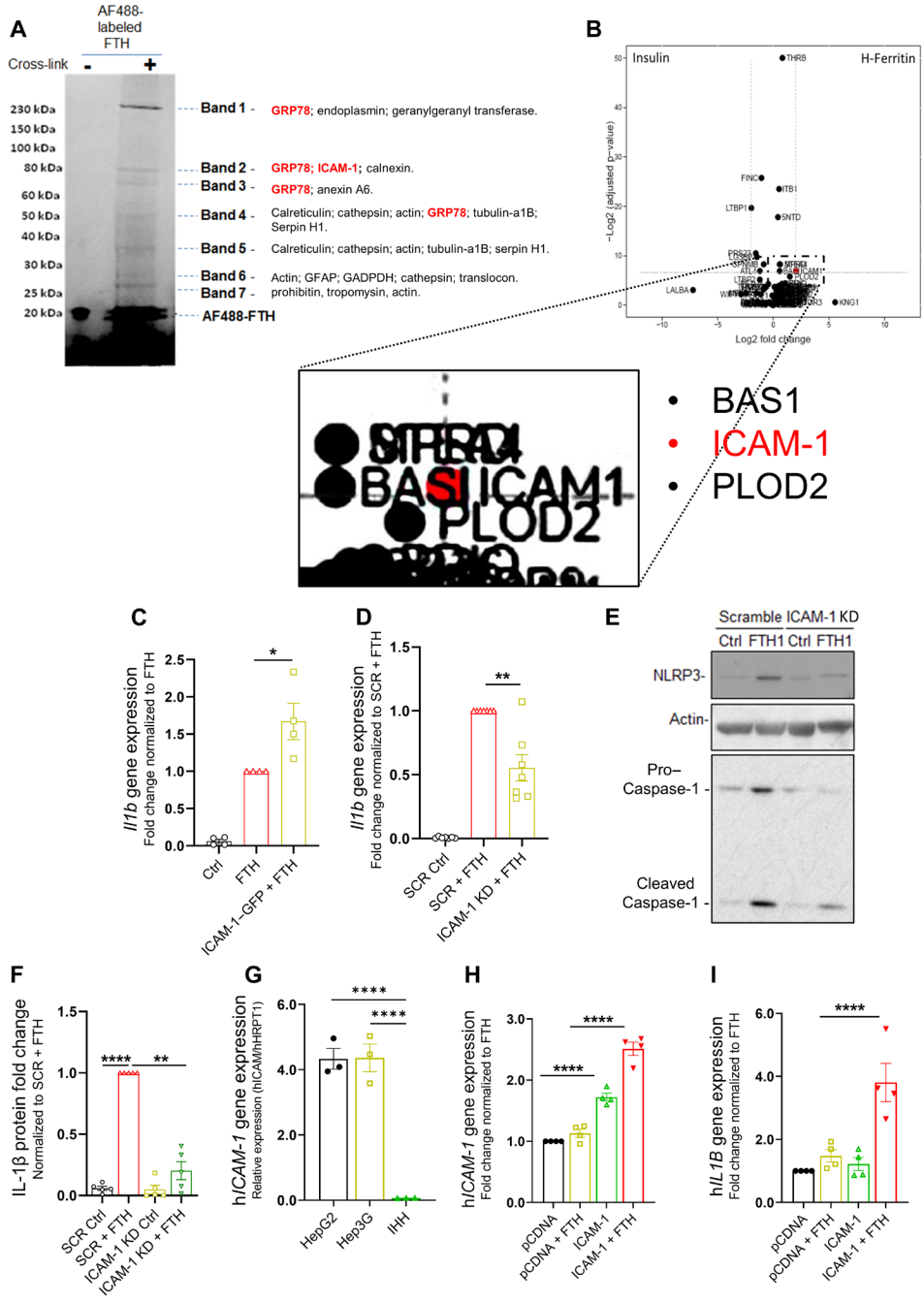

Fig. 2. ICAM-1 is the FTH signaling receptor that mediates inflammasome activation in rat and human HSCs. (**A**) SDS electrophoresis gel showing bands containing AF488–labeled FTH-binding proteins, identified by MS in primary rat HSCs. Gel is representative of $n = 3$ independent experiments. (**B**) Proteins identified by ligand-receptor glycocapture that bind to FTH as potential candidates for the FTH receptor in primary rat HSCs. $n = 3$ independent experiments. Enlarged region of the ligand-receptor glycocapture volcano plot highlights ICAM-1 as the only statistically significant FTH-binding protein (red circle). (**C**) *Il1b* mRNA expression (fold change normalized to that in the FTH group) in primary rat HSCs transfected with GFP (control) or ICAM-1–GFP overexpression plasmids 24 hours before treatment with FTH for 2 hours. $n = 4$ independent experiments. (**D**) *Il1b* mRNA expression (fold change normalized to that in the SCR + FTH group) in primary rat HSCs transfected with scrambled siRNA (SCR) or ICAM-1 KD siRNA 24 hours before treatment with FTH for 2 hours. $n = 7$ independent experiments. (**E**) Western blot showing NLRP3 and caspase-1 in primary rat HSCs transfected with scrambled (SCR) or ICAM-1 siRNA and treated with vehicle (Ctrl) or FTH for 24 hours. Actin is a loading control. $n = 3$ independent experiments. (**F**) ELISA analysis of IL-1β secretion after ICAM-1 KD rat primary HSCs treated with FTH for 24 hours. $n = 5$ independent experiments. (**G**) Comparative expression of endogenous *ICAM-1* relative to *HPRT1* in human liver and HCC cell lines HepG2, Hep3G, and IHH. $n = 3$ independent experiments. (**H** and **I**) Expression of *ICAM-1* (H) and *IL1B* (I) in IHH cells that were transfected with *ICAM-1* or empty vector (pCDNA 3.0) for 24 hours and treated with FTH for 2 hours. Changes in mRNA expression are expressed as fold change relative to *HPRT1*. $n = 4$ independent experiments. All results in bar graphs are presented as mean (fold change) ± SEM. Statistical analysis was performed using a repeated measures one-way ANOVA with Šídák's multiple comparisons test or paired Student's *t* test, where $P \leq 0.05$ was considered statistically significant. *$P \leq 0.05$, **$P \leq 0.01$, and ****$P \leq 0.0001$.

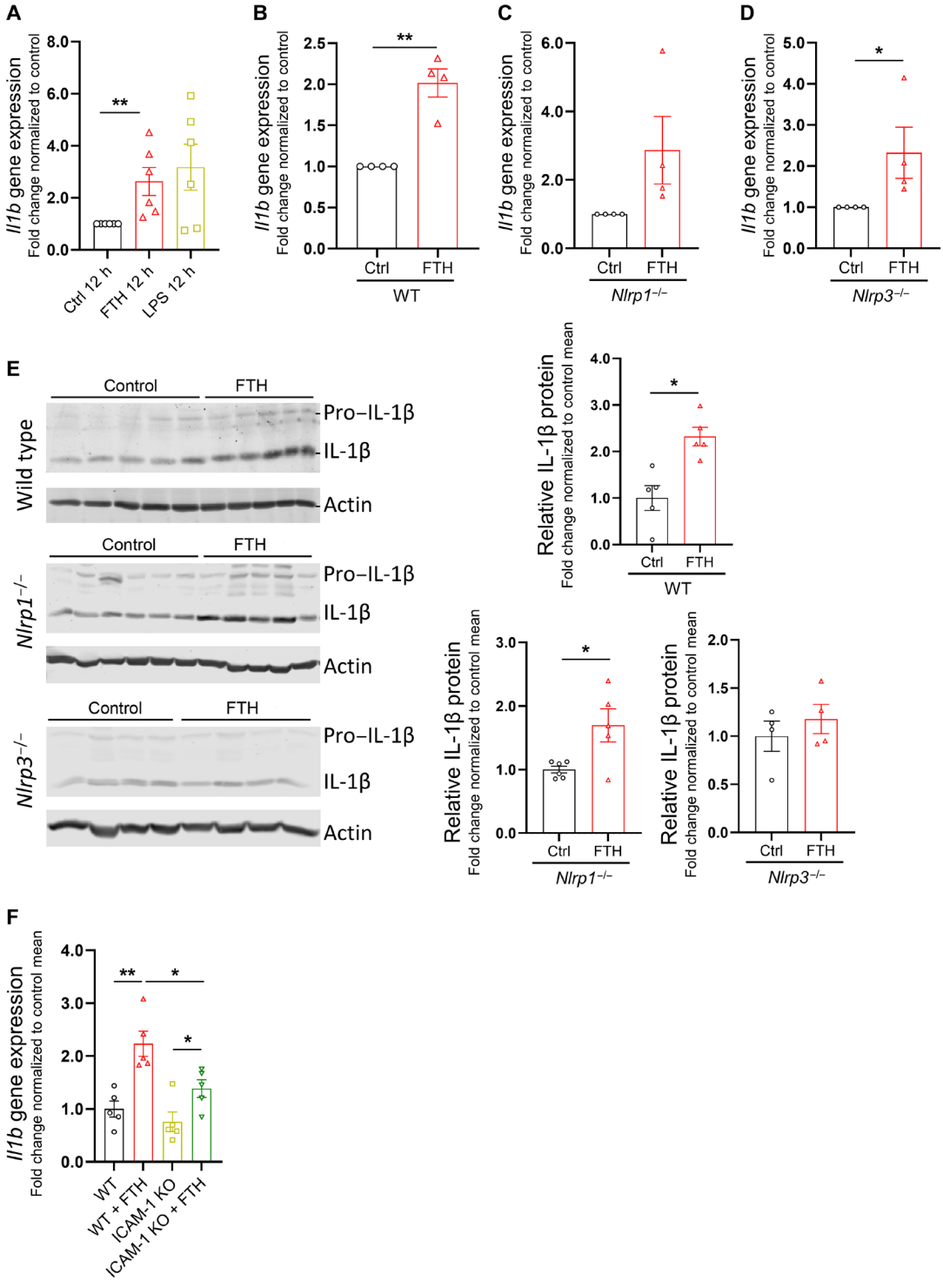

Fig. 3. FTH stimulates inflammasome activation and IL-1β synthesis in liver slices. (**A**) *Il1b* expression in precision-cut liver slices from WT mice treated ex vivo with FTH or LPS for 12 hours or untreated. $n = 6$ mice per treatment group. (**B** to **D**) *Il1b* expression in precision-cut liver slices from WT (B), *Nlrp1*$^{-/-}$ (C), or *Nlrp3*$^{-/-}$ (D) mice treated ex vivo with FTH for 12 hours or untreated. $n = 4$ mice per treatment group. (**E**) Representative Western blot for pro–IL-1β and mature IL-1β in precision-cut liver slices from WT, *Nlrp1*$^{-/-}$, and *Nlrp3*$^{-/-}$ mice treated ex vivo with FTH for 12 hours. Mature IL-1β protein was quantified relative to the actin loading control. Each lane represents one liver slice; slices were obtained from three mice per treatment group. Quantification of mature IL-1β is based on three blots. (**F**) *Il1b* expression in precision-cut liver slices from *Icam1*$^{-/-}$ mice and matching WT colony controls treated ex vivo with FTH for 12 hours. $n = 5$ mice per treatment group. All results in bar graphs are presented as mean (fold change) ± SEM. Statistical analysis was performed using a paired Student's *t* test (A to D) or an unpaired Student's *t* test (E and F), where $P \leq 0.05$ was considered statistically significant. *$P \leq 0.05$ and **$P \leq 0.01$.

Although precision-cut liver slices provide whole-tissue physiological relevance to our observation of FTH-induced, ICAM-1–mediated NLRP3 inflammasome activation, a key limitation of this technique is the relative inability to identify the cellular source of inflammation within the liver slices. Others have likewise shown that immunohistochemical assessment of liver pathobiology is extremely challenging in liver slice studies (*22*). Therefore, it remains possible that other liver cell populations, in addition to HSCs, may also contribute to FTH-induced inflammation in precision-cut liver tissue slices.

FTH–ICAM-1 signaling in HSCs is mediated by CCP endocytosis

To understand the cellular events underlying the transduction of FTH signaling, we examined the involvement of the plasma membrane and the endocytic system of primary rat HSCs after exposure to FTH. Confocal visualization of the plasma membrane cholesterol-enriched lipid domains with the cationic dye Di-4-ANEPPDHQ, which responds in submillisecond membrane potential changes (*23*, *24*) in comparison to the basal fluorescence profile of the HSC plasma membrane (0 to 90 s), showed that FTH induced a transient change of the plasma membrane potential within seconds, consistent with reorganization of the plasma membrane (Fig. 4A). Accordingly, when primary rat HSCs were exposed to FTH for 30 s, caveolin-1 (CAV1), a marker of lipid raft subtype caveolae (*25*), exhibited a differential flotation in sucrose gradient of plasma membrane fractions versus untreated HSCs (Fig. 4B), indicative of structural reorganization of plasma membrane microdomains. Moreover, inhibition of lateral diffusion of the plasma membrane proteins of primary rat HSCs using α-cyclodextrin, which does not interfere with cholesterol (*26*), reduced FTH-induced *Il1b* expression (Fig. 4C). Together, these data suggest that plasma membrane organization plays an important role in the transduction of FTH-induced proinflammatory signaling in HSCs.

Signaling by plasma membrane receptors often involves internalization and trafficking through endosomal compartments (*27*, *28*). We previously reported that FTH is internalized by primary rat HSCs (*18*). To shed light on the contribution of major endocytic pathways, such as CCP and caveolae endocytosis, to the signal transduction initiated by FTH–ICAM-1, we used Dyngo4a (an inhibitor of dynamin-2–dependent caveolae and CCP endocytosis), and PitStop2 (specifically prevents CCP endocytosis) (*29*, *30*). Dyngo4a and PitStop2 inhibit epidermal growth factor receptor (EGFR) endocytosis, trapping it at the plasma membrane in cancer cells. In this context, Dyngo4a has been shown to enhance the cytotoxicity of antibody therapeutics directed at EGFR by maintaining EGFR at the plasma membrane, which allows more effective natural killer cell–mediated, antibody-dependent cellular cytotoxicity (ADCC) in vitro. Although Dyngo4a has not been tested in humans, the potential therapeutic utility of CCP inhibitors has been demonstrated by prochlorperazine, which enhances ADCC in cancer (*31*). Both Dyngo4a and PitStop2 inhibited FTH-mediated *Il1b* expression in primary rat HSCs (Fig. 4D). Transient (partial) KD of clathrin (using *CLTC* as the target gene) using specific siRNA (Fig. 4E) or inhibition of CCP endocytosis with ikarugamycin (*32*) in primary rat HSCs treated with FTH (Fig. 4F) recapitulated these results. To examine the role of caveolae-mediated endocytosis in FTH signaling, we used β-methyl cyclodextrin (MCD), which sequesters free cholesterol in the plasma membrane and disrupts plasma membrane lipid rafts, including caveolae. MCD exacerbated the FTH-induced increase in *Il1b* expression in primary rat HSCs (Fig. 4G). Together, these results suggest that FTH stimulates *Il1b* mRNA expression in a dynamin-2– and CCP endocytosis–dependent manner.

In cells treated with PitStop2, confocal imaging showed that FTH enhanced the colocalization of ICAM-1 and clathrin at the plasma membrane and within intracellular compartments (fig. S4). This colocalization diffused over time until ICAM-1 and clathrin labeling at the plasma membrane returned to a basal state 2 hours after FTH treatment (fig. S4). Cross-section quantification of cell edge to cell body ratios of ICAM-1 labeling showed that FTH induced ICAM-1 internalization and that both Pitstop2 and Dyngo4a caused retention of ICAM-1 (in FTH-treated primary rat HSCs), at the plasma membrane, although for PitStop2, the quantification did not reach statistical significance (Fig. 4H). PitStop2 inhibited the expression of FTH-induced *Il1b* mRNA in primary rat HSCs overexpressing ICAM-1–GFP (versus GFP) (Fig. 4I) and reduced FTH-induced phosphorylation of p65 (P-p65), a marker of NF-κB activation (Fig. 4J and fig. S9A), and induction of NLRP3 (Fig. 4K and fig. S9B). PitStop2 did not prevent caspase-1 cleavage in response to either FTH or LPS (Fig. 4K). These data suggest that in primary rat HSCs, CCP constitutes the specific plasma membrane domain for FTH–ICAM-1 priming, but not activation, of the NLRP3 inflammasome.

FTH–ICAM-1 signaling in HSCs involves the actin cytoskeleton

In agreement with the involvement of the actin cytoskeleton in mediating CCP endocytosis (*33*, *34*), inhibition of actin polymerization by latrunculin-A suppressed FTH-stimulated *Il1b* expression in rat HSCs (fig. S5A). However, disruption of the microtubule cytoskeleton by nocodazole had no effect in FTH-induced *Il1b* expression (fig. S5B). Phalloidin labeling of actin filaments revealed that 2- to 5-min treatment with FTH, but not FTL, induced a transient reorganization of the actin cytoskeleton, reflected by the reduction in the density of actin filaments (fig. S5C), and tubulin staining showed that FTH did not alter the microtubule cytoskeleton (fig. S5D). Either repression of CCP endocytosis using PitStop2 or inhibition of actin polymerization using latrunculin-A prevented FTH-induced activation of mitogen-activated protein kinase and extracellular signal-regulated kinase pathway (fig. S5E), further demonstrating the importance of the actin cytoskeleton and clathrin-mediated endocytosis in FTH signaling. Confocal imaging showed that latrunculin-A prevented FTH-induced ICAM-1 redistribution into the cytosol and caused its accumulation at the plasma membrane (fig. S5F). Accordingly, exposing primary rat HSCs to latrunculin-A at different intervals (1 to 30 min) after FTH stimulation still prevented induction of *Il1b* expression (fig. S5G). These results suggest that regulation of FTH signaling by the actin cytoskeleton may occur at different compartmentalization levels, including at the early and late endosomes. Actin cytoskeleton organization is directly modulated by the small guanosine triphosphatases RhoA1, Rac1, and Cdc42 (*33*, *34*). Cdc42 and Rac1 inhibitors (ML141 and NSC23766, respectively), but not the RhoA1 inhibitor C3 transferase (C3T), reduced FTH-induced *Il1b* gene expression (fig. S5, H and I) and the increase in NLRP3 protein (fig. S5J). Thus, our data suggest that the actin cytoskeleton aids in facilitating FTH-induced pro-inflammatory signaling in HSCs through Cdc42 and Rac1.

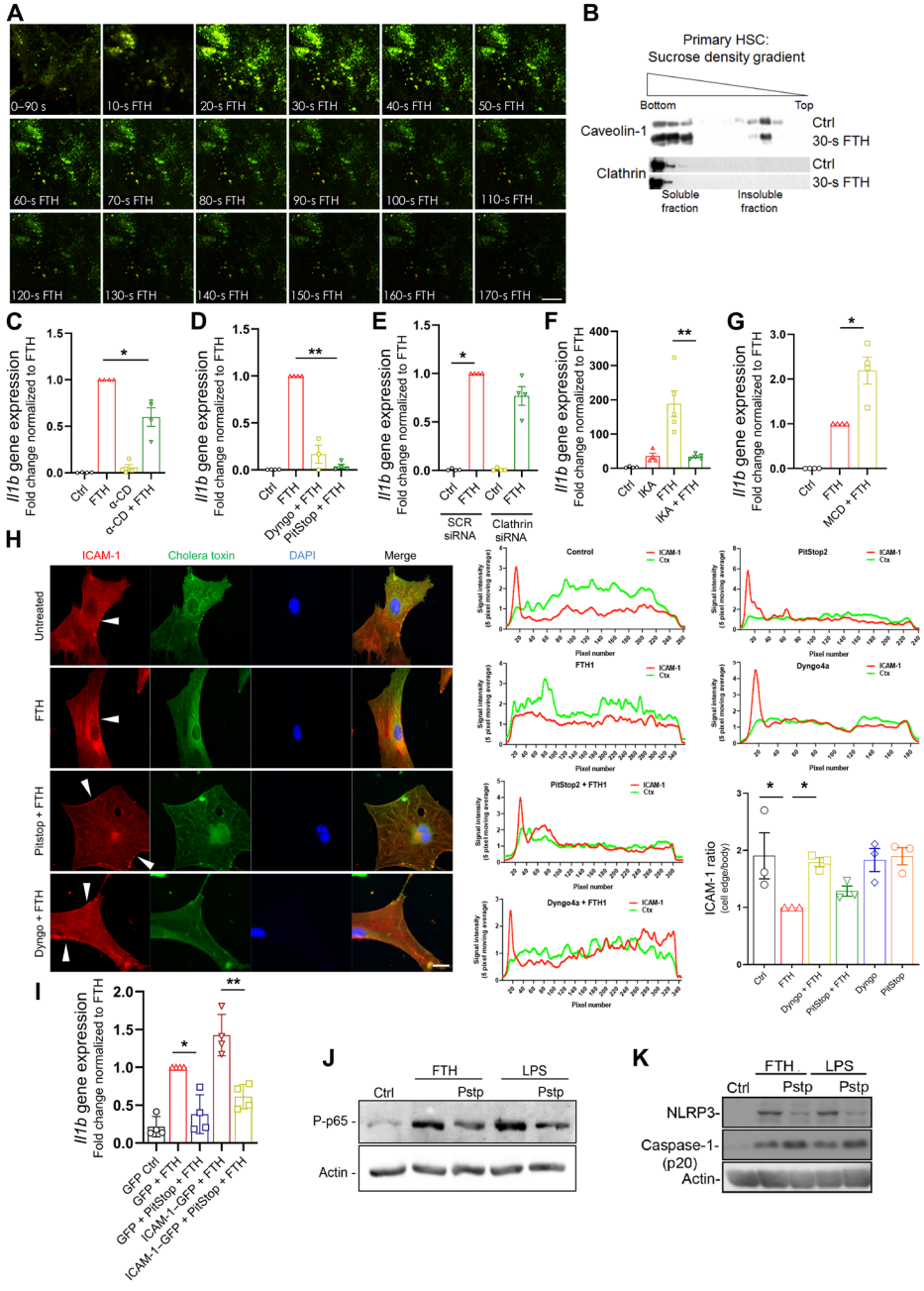

Fig. 4. FTH–ICAM-1–induced signaling is mediated by CCP endocytosis requiring the actin cytoskeleton. (**A**) Time course of Di-4-ANEPPDHQ labeling of primary rat HSC plasma membranes before (0 to 90 s) and after (10 to 180 s) FTH stimulation. Images are representative of $n = 7$ independent experiments. Scale bar, 20 μm. (**B**) Representative Western blot of the flotation of CAV1 (lipid raft marker) and clathrin in cellular fractions of primary rat HSCs separated by discontinuous sucrose gradient ultracentrifugation. $n = 3$ independent experiments. (**C** to **G**) *Il1b* expression after 2 hours of FTH stimulation in primary rat HSCs pretreated with α-cyclodextrin (α-CD) to limit lateral diffusion of plasma membrane proteins (C), treated with the endocytosis inhibitors Dyngo4a or PitStop2 (D), transfected with control (SCR) or clathrin siRNA (E), pretreated with the endocytosis inhibitor ikarugamycin (IKA), or treated with β-methyl cyclodextrin (MCD) to disrupt lipid raft microdomains (G). $n = 3$ (D), $n = 4$ (C, E, and G), or $n = 5$ (F) independent experiments. (**H**) Immunofluorescence for ICAM-1 in primary rat HSCs also labeled with the plasma membrane marker cholera toxin (Ctx). Cells were treated with FTH for 2 min, along with either Dyngo4a or PitStop2. Scale bar, 20 μm. Cell edge/cell body ratios of ICAM-1 labeling were derived from the quantification of cross sections from the images. Cells treated with either Dyngo4a or PitStop2 but not stimulated with FTH were used as experimental controls. $n = 10$ to 12 cross sections from three independent experiments for each group. (**I**) *Il1b* expression in primary rat HSCs transfected with GFP (control) or ICAM-1–GFP overexpression plasmids, treated with PitStop2 or vehicle with FTH stimulation for 2 hours. $n = 4$ independent experiments. (**J**) Representative Western blot showing phosphorylated p65 in primary rat HSCs treated with PitStop2 with FTH stimulation for 2 hours. Actin is a loading control. Blot is representative of $n = 3$ independent experiments. (**K**) Representative Western blot showing NLRP3 and cleaved caspase-1 (p20 fragment) in primary rat HSCs treated with PitStop2 or vehicle with FTH or LPS stimulation for 24 hours. Blot is representative of $n = 4$ independent experiments. Results in bar graphs are presented as mean (fold change) ± SEM. Statistical analysis was performed using a repeated measures one-way ANOVA with Šídák's multiple comparisons test or paired Student's *t* test, where $P \leq 0.05$ was considered statistically significant. *$P \leq 0.05$ and **$P \leq 0.01$.

Early endosomes are platforms for FTH signaling in HSCs

PitStop2 and Dyngo4a inhibit CCP endocytosis by preventing clathrin detachment from CCP without affecting CCP integrity, resulting in CCP accumulation at the plasma membrane (*29*, *30*). Therefore, if FTH–ICAM-1 signaling originated at the plasma membrane, then PitStop2 and Dyngo4a treatment should increase FTH-induced *Il1b* expression; however, we observed inhibition with these reagents (Fig. 4D). Therefore, we hypothesized that FTH–ICAM-1 signaling may occur in intracellular compartments after CCP-dependent endocytosis rather than at the plasma membrane. To address the potential involvement of different endosome compartments in the regulation of FTH-induced proinflammatory signaling in primary rat HSCs, we overexpressed fluorescently tagged WT and mutant [constitutively active and dominant negative (DN)] forms of key endosome regulatory proteins (fig. S6). In primary rat HSCs, overexpression of full-length (FL) WT protein regulators of the early endosomes, RAB5 (GFP-RAB5) or early endosome antigen 1 (RFP-EEA1), but not phosphotyrosine interacting with PH domain and leucine zipper 1 (RFP-human APPL1), significantly augmented FTH-induced expression of *Il1b* transcripts (Fig. 5A). Overexpression of the FL and constitutive active (CA) isoforms of the recycling endosome protein RAB11 increased FTH-induced *Il1b* transcripts in primary rat HSCs (Fig. 5, A and B), suggesting that the recycling endosome compartment may promote FTH signaling through exocytosis of ICAM-1. Overexpression of the CA mutant forms of RAB5 (RAB5 Q79L) or RAB7 (RAB7 Q71L) did not alter FTH-induced *Il1b* transcript expression (Fig. 5B). However, accumulation and defective flux of early endosome cargo toward the late endosome compartment by overexpression of DN RAB5 (GFP-RAB5 S34N) enhanced FTH-induced *Il1b* expression, whereas overexpression of the FL or the DN mutant of RAB7 (RAB7 T22N) had no effect on FTH-induced *Il1b* expression (Fig. 5C). Looking at NLRP3 protein, overexpression of FL-RFP-EEA1, FL-RFP-human-APPL1, or FL-GFP-RAB5 increased NLRP3 protein (Fig. 5D). Analysis of FTH trafficking in FTH-treated primary rat HSCs initially showed the colocalization of FTH with the plasma membrane marker ZO-1 after 5 s and subsequent colocalization with the early endosome marker EEA1 at 5 and 15 min (fig. S7A), which supports the involvement and movement of FTH from the plasma membrane to the early endosome. Furthermore, GFP-RAB7 overexpression increased NLRP3 protein in FTH-treated primary rat HSCs (Fig. 5D). Together, these data suggest a model in which signaling at early endosomes promotes the induction of *Il1b* expression, and the increase in NLRP3 and the late endosome-lysosome compartment may also participate in inflammasome activation during FTH stimulation.

These results suggest that early endosomes are the most likely cellular compartment for FTH signaling. Early endosomes have emerged as signaling platforms in other cellular contexts (*28*, *35*). To assess the involvement of early endosomes in FTH signaling, we sought to deplete HSCs of early endosomes. Partial KD of *Rab5a* ($59.80 \pm 0.14\%$), *Rab5b* ($51.10 \pm 0.06\%$) and *Rab5c* ($68.00 \pm 0.09\%$) (*Rab5a-c* KD) in primary rat HSCs using siRNAs (fig. S7B) (*36*) caused a significant depletion of early endosomes and reduced the size of $EEA1^+$ (Fig. 5E) and $RAB5^+$ early endosomes (fig. S7C), without affecting $APPL1^+$ early endosomes (fig. S7C). Accordingly, and without impairing *Il1b* expression (Fig. 5F), *Rab5a-c* KD blunted FTH stimulation of NLRP3 protein (Fig. 5G) and significantly reduced IL-1β secretion (Fig. 5H). In addition, when RAB5 was overexpressed in *Rab5a-c* KD primary rat HSCs in the absence of FTH, *Il1b* expression was not induced, ruling out an FTH-independent function of early endosomes on *Il1b* expression (Fig. 5I). However, overexpression of RAB5 in FTH-treated *Rab5* KD primary rat HSCs, restored FTH-induced *Il1b* expression by two- to threefold, revealing that FTH signaling may be a saturable process that is not responsive to progressive increases in the amount of RAB5 overexpression (Fig. 5I).

FTH-induced activation of the inflammasome is facilitated by lysosomal destabilization

Priming and activation of inflammasomes are triggered by a range of stimuli, including molecules such as DAMPs, which are damage signaling molecules released from ischemic tissues and from damaged and dying cells. These are usually intracellular molecules, such as adenosine 5′-triphosphate and uric acid crystals, that become damage signaling molecules when in the extracellular environment (*37*). Intracellular FTH released into the extracellular environment in response to cellular damage could potentially act as a DAMP. Activation of the inflammasome by DAMPs can involve secondary factors, such as reactive oxygen species (ROS), Ca^{2+} signaling, and lysosomal destabilization, downstream of these signals (*38*–*40*). Primary rat HSCs exhibited a modest increase in FTH-induced ROS (Fig. 6A), and thus, we speculate that enhanced ROS production may constitute a possible activation signal causing the assembly and activation of the inflammasome in response to extracellular FTH. We also observed that different inhibitors of adenosine triphosphatase pumps in late endosomes (including bafilomycin, chloroquine, and monensin) reduced or prevented the expression of FTH-induced *Il1b* mRNA (Fig. 6, B and C), suggesting that endosome-lysosome trafficking may be required for FTH signaling. Although bafilomycin did not appear to affect ICAM-1 trafficking, chloroquine caused accumulation of ICAM-1 at the plasma membrane (fig. S8), implying that the effects of inhibiting late endosome-lysosome function on FTH signaling are not a consequence of bafilomycin, chloroquine, or monensin targeting ICAM-1 per se.

Previous studies have suggested that endogenous or exogenously derived ferritin can lead to lysosomal leak or disruption (*41*, *42*). Therefore, we assessed whether ROS or lysosomal fragility may act as possible inflammasome-activating signals in FTH-treated primary rat HSCs. CA-074me, an irreversible inhibitor of the lysosomal cysteine protease cathepsin-B, which is released in response to lysosomal destabilization and triggers inflammasome activation, reduced the FTH-induced increase in NLRP3 protein (Fig. 6D) and IL-1β secretion (Fig. 6E). However, MitoTEMPO (a specific inhibitor of mitochondrial-derived ROS) had no significant effect (Fig. 6, D and E). Therefore, these results suggest that FTH stimulates NLRP3 inflammasome assembly and activation by inducing lysosomal fragility and not through mitochondrial-derived ROS.

To summarize our observations from this study, we propose that FTH acts as a DAMP that stimulates inflammasome activation in HSCs after binding to and being endocytosed with ICAM-1 (Fig 6F). In combination with our previously published observations of FTH-induced PKCζ and NF-κB signaling (*7*), these findings shed light on the cellular and molecular mechanisms that result in FTH–ICAM-1–induced NLRP3 inflammasome activation and IL-1β maturation and secretion in HSCs. We speculate that this contributes to

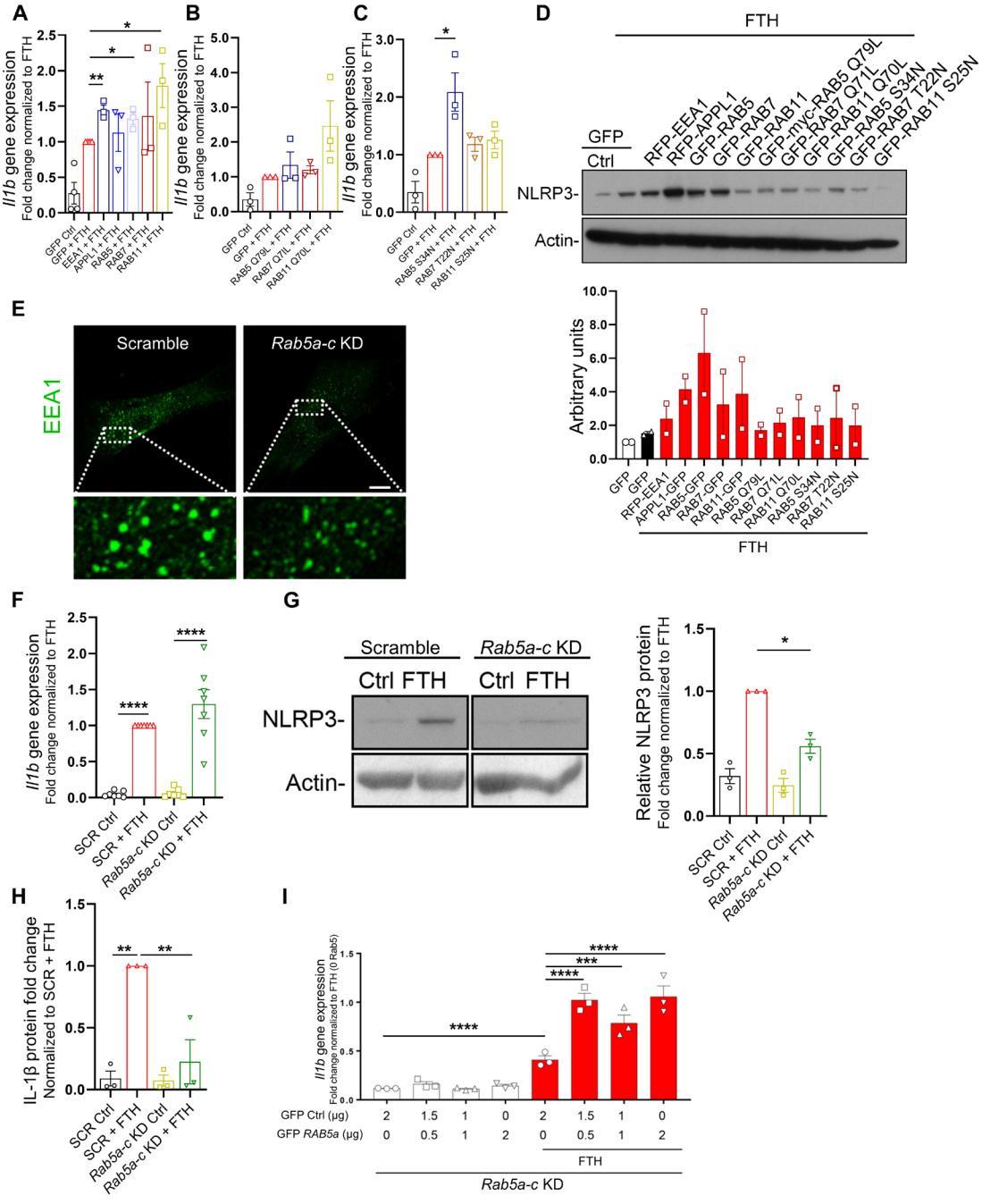

Fig. 5. Early endosomes are the signaling platform for FTH-induced inflammasome activation. (**A**) *Il1b* expression in FTH-treated (2 hours) primary rat HSCs (2 hours) overexpressing empty GFP vector and FL WT RFP-tagged EEA1 (EEA1), RFP-tagged APPL1 (APPL1), GFP-tagged RAB5 (RAB5), GFP-tagged RAB7 (RAB7), or GFP-tagged RAB11 (RAB11). $n = 3$ independent experiments per group. (**B**) *Il1b* gene expression in FTH-treated (2 hours) primary rat HSCs overexpressing empty GFP vector or the constitutively active RAB mutants pEGFP-C3-myc-RAB5 Q79L (RAB5 Q79L), pEGFP-C-RAB7 Q71L (RAB7 Q71L), or pEGFP-C3-RAB11 Q70L (RAB11 Q70L). $n = 3$ independent experiments per group. (**C**) *Il1b* gene expression in FTH-treated (2 hours) primary rat HSCs overexpressing empty GFP vector or the DN Rab mutants pEGFP-C2-RAB5 S34N (RAB5 S34N), pEGFP-C-RAB7 T22N (RAB7 T22N), and pEGFP-C3-RAB11 S25N (RAB11 S25N). $n = 3$ independent experiments per group. (**D**) Representative Western blot and quantitation of NLRP3 in FTH-treated (24 hours) primary rat HSCs overexpressing GFP or FL forms of the indicated proteins. Actin is a loading control. Blot is representative of $n = 2$ independent experiments. (**E**) Confocal imaging of the early endosomal marker EEA1 in primary rat HSCs transfected with scrambled siRNA or siRNA pool targeting *Rab5a-c*. $n = 3$ independent experiments. Scale bar, 20 μm. (**F** to **H**) Primary rat HSCs were transfected with scrambled siRNA (SCR) or siRNA pool targeting *Rab5a-c* and treated with FTH for 24 hours or not. *Il1b* expression (F), NLRP3 protein relative to the actin loading control (G), and IL-1β secretion into the medium (H) were quantified. $n = 7$ (F) or $n = 3$ (G and H) independent experiments per group. (**I**) *Il1b* expression in primary rat HSCs with siRNA-mediated *Rab5a-c* KD (Rab5 KD) and transfected with equal amounts of plasmids (2 μg) encoding either GFP or GFP-RAB5 before treatment with FTH for 2 hours. $n = 3$ independent experiments per group. Results in bar graphs are presented as mean (fold change) ± SEM. Statistical analysis was performed using a repeated measures one-way ANOVA with Šídák's multiple comparisons test or paired Student's *t* test, where $P \leq 0.05$ was considered statistically significant. *$P \leq 0.05$, **$P \leq 0.01$, ***$P \leq 0.001$, and ****$P \leq 0.0001$.

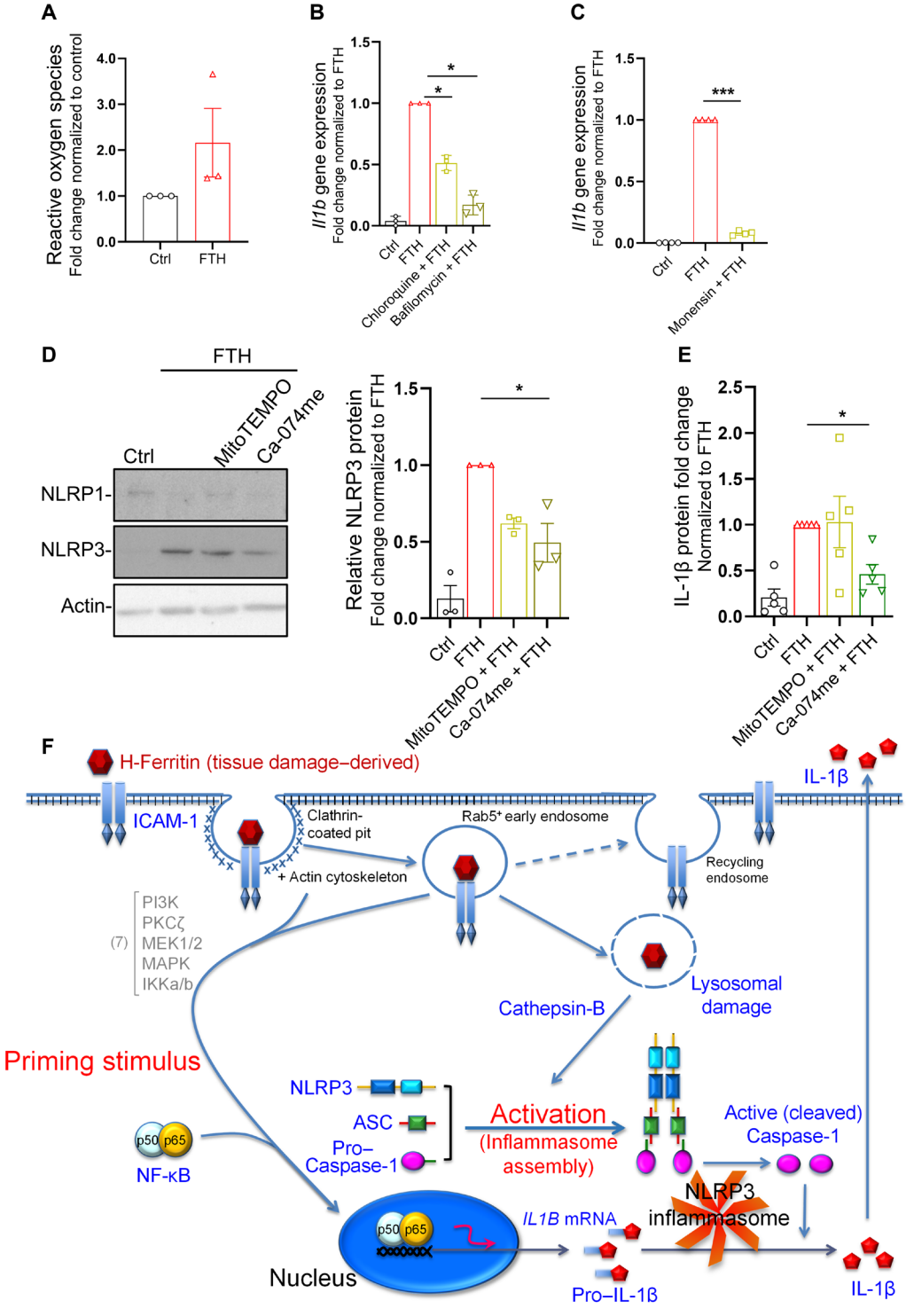

Fig. 6. FTH stimulates inflammasome activation in rat HSCs by destabilizing lysosomes. (**A**) ROS synthesis in primary rat HSCs treated with FTH for 2 hours. $n = 3$ independent experiments. (**B** and **C**) *Il1b* expression in primary rat HSCs treated with inhibitors of late endosome/lysosome acidification chloroquine, bafilomycin (B), or monensin (C) with FTH stimulation for 2 hours. $n = 3$ (B) or 4 (C) independent experiments. (**D**) Representative Western blots for NLRP1 and NLRP3 and quantification of NLRP3 in FTH-treated (24 hours) primary rat HSCs exposed to either the mitochondrial ROS synthesis inhibitor MitoTEMPO or the cathepsin-B inhibitor CA-074me. $n = 3$ independent experiments. (**E**) IL-1β secretion as measured by ELISA in FTH-treated (24 hours) primary rat HSCs exposed to either MitoTEMPO or CA-074me. $n = 5$ independent experiments. (**F**) Proposed cell signaling mechanisms of FTH–ICAM-1–induced inflammasome activation and subsequent IL-1β secretion in HSCs. Results in bar graphs are presented as mean (fold change) ± SEM. Statistical analysis was performed using a repeated measures one-way ANOVA with Šídák's multiple comparisons test or paired Student's *t* test, where $P \leq 0.05$ was considered statistically significant. *$P \leq 0.05$ and ***$P \leq 0.001$. PI3K, phosphatidylinositol 3-kinase; MAPK, mitogen-activated protein kinase; MEK1/2, MAPK kinase 1/2; IKKa/b, IκB kinase a/b.

hepatic inflammation, a key causal process underlying hepatic fibrogenesis associated with chronic liver disease.

DISCUSSION

The world is facing an exponential increase in the incidence of chronic liver disease (*43*). Chronic liver disease is the progressive deterioration of liver function, which can ultimately lead to fibrosis, cirrhosis, and the development of primary liver cancer, usually hepatocellular carcinoma (*44*). Chronic liver diseases result from damage to hepatocytes that then triggers hepatic inflammation and fibrogenesis. Although hepatic inflammation and fibrogenesis are part of normal tissue repair responses, these processes, when prolonged, contribute to the progression of chronic liver disease through the destruction and replacement of functional liver tissue with inactive scar tissue. In the context of hepatic inflammation, the identification of ICAM-1 as the FTH signaling receptor responsible for activation of the NLRP3 inflammasome and secretion of IL-1β in primary rat HSCs in response to FTH constitutes an advance both in understanding the mechanism of hepatic inflammation and for the search for potential therapeutic targets to ameliorate inflammation and therefore slow or halt this key component of chronic liver disease progression.

Our conclusions are supported by data obtained from a range of experimental models, including primary rat HSCs, human HSCs, and ex vivo precision-cut liver tissue from WT mice and mice deficient in ICAM1, NLRP1, or NLRP3. Mechanistically, to understand the transduction of the proinflammatory cascades underlying FTH–ICAM-1 interaction in disease, we have dissected the series of cellular and molecular events that promote the propagation of FTH-induced signaling from the plasma membrane to the assembly and activation of the inflammasome. This includes the involvement of CCP endocytosis, Cdc42/Rac1-induced actin cytoskeleton reorganization, and dynamic changes in plasma membrane organization for the transcriptional responses that prime the cell for inflammasome activation. In addition, our data demonstrate that $RAB5^+$ early endosomes, rather than the HSC plasma membrane, were the main physical platform associated with triggering FTH–ICAM-1–induced signaling, resulting in activation of the NLRP3 inflammasome and secretion of IL-1β. We have also revealed the dependence of FTH proinflammatory signaling on the induction of lysosomal fragility and cathepsin-B release for generation of the activating signal that triggers assembly of the inflammasome, caspase-1 activation, and cleavage and secretion of mature IL-1β protein.

Our study has also identified potential HSC-specific interactions between the NLRP components of the inflammasome. Whereas FTH induces only NLRP3 protein in primary rat HSCs, KD of NLRP1 had a significant inhibitory effect on IL-1β secretion similar to that observed in response to NLRP3 depletion. This suggests that FTH-induced secretion of active IL-1β by HSCs may involve coregulation or cooperation between multiple NLRP inflammasome subsets. Whether this is a cellular event specific to HSCs or whether it can be observed in other cell types within the liver warrants further investigations.

In addition, our study provides initial insights into the potential existence of binding protein adaptors or coregulatory molecules that may act in concert with ICAM-1 to facilitate FTH proinflammatory signaling. This is the case for GRP78, which appeared to be required for the FTH-induced assembly of the inflammasome and the secretion of IL-1β but did not play a role in the induction of *Il1b* expression that primes the cell for inflammasome activation. Given the ubiquitous nature of ICAM-1 on cells, such protein adaptors or coregulatory molecules may provide cellular specificity for FTH–ICAM-1 signaling.

In conclusion, we postulate that under pathophysiological conditions, liver damage and apoptosis of hepatic cells cause the release of increased concentrations of hepatocellular-derived ferritin into the extracellular hepatic microenvironment (*45*). This imparts a paracrine proinflammatory response on HSCs mediated by the interaction of FTH with ICAM-1 at the plasma membrane, which drives hepatic inflammation. We cannot rule out the possibility that FTH also activates inflammasomes in other liver cell types. Liver sinusoidal endothelial cells produce high amounts of ICAM-1, have the capacity to produce IL-1β and IL-6 under certain conditions (*46*), and are involved in inflammation mediated by lymphocyte function–associated antigen 1 (LFA-1) binding to ICAM-1 (*47*). Cholangiocytes and hepatocytes both express ICAM-1 in conditions of hepatic injury (*48*). However, hepatocyte ICAM-1 distribution is mainly limited to the plasma membrane domains surrounding bile canaliculi (*49*). Regarding this, our experiments in IHH cells that express low endogenous *ICAM1* suggested that FTH might stimulate IL-1β and sterile inflammation in hepatocytes under pathophysiological conditions that increase hepatocyte ICAM-1 content. Also, although hepatic macrophages are known to secrete inflammatory cytokines, we have previously shown they do not exhibit specifically bind to tissue ferritin (*18*). Because it is possible that FTH may play a role through ICAM-1 in other cell types, further investigations are warranted to assess the implication of this pathway of inflammasome activation in other hepatic cells in chronic liver disease.

Although we demonstrated the potential pathophysiological relevance of our proposed FTH–ICAM-1–activated, NLRP3 inflammasome–induced IL-1β secretion in in vitro cell culture and in precision-cut ex vivo liver slices from WT, ICAM-1 knockout, NLRP-3 knockout, and NLRP-1 knockout mice, we were limited in our investigation by the lack of appropriate in vivo murine models for the loss of ferritin or pathophysiological increases in the release of ferritin. Specifically, the embryonic lethality of FTH knockout mice (*50*) prevented the validation of the effect of FTH on ICAM-1 signaling–induced NLRP3 inflammasome function in mouse models of liver inflammation and fibrosis. We were also limited by the lack of availability of a floxed ICAM-1 mouse model that would have allowed us to generate HSC-specific ICAM-1 knockout mice to more accurately evaluate the importance of FTH–ICAM-1 interactions for the inflammasome-activated secretion of IL-1β in HSCs.

MATERIALS AND METHODS

Primary HSC isolation and ferritin treatments

Studies were performed with approval from the QIMR Berghofer Medical Research Institute Animal Ethics Committee and in compliance with Australian regulatory guidelines (ethics numbers: A0102-00-012 and A1212-620 M). Primary rat HSCs were isolated from normal male Sprague-Dawley rats (aged 9 to 18 months old and 600 to 1000 g in body weight) by sequential pronase and collagenase perfusion of livers and then cultured on plastic 12-well plates and grown in medium 199 (Invitrogen) supplemented with 10% calf serum + 10% horse serum, and penicillin/streptomycin (100 U and 100 μg/ml, respectively) to induce an activated phenotype, as we previously described (*7*). Twenty-four hours before experimentation, HSCs were washed and cultured in serum-free

M199. Primary rat HSCs were then treated with recombinant human H-ferritin (FTH; a kind gift from P. Arosio and M. Poli, University of Brescia, Italy). Human and rat FTH have high protein sequence homology of (97%) using BLASTp. Recombinant FTH and FTL (10 nM, unless otherwise stated) were prepared as described (*51*), and any potential contaminating LPS was removed using the Pierce High Capacity Endotoxin Removal Spin Column Kit (Thermo Fisher Scientific, catalog no. 88273) following the manufacturer's instructions. Recombinant FLAG-FTH (10 nM) (catalog no. RC209845) and FLAG-FTL (10 nM) (catalog no. RC203296) were generated in human kidney HEK cells, purchased from Origene (and referred to as human-generated FTH and FTL). Five-day culture-activated primary rat HSCs were routinely used except where indicated.

Transgenic mouse lines

ICAM-1–deficient mice lacking the entire coding region of the ICAM-1 gene ($Icam1^{tm1Alb}$) have been previously created (*52*) and backcrossed on to the C57BL/6J background for more than 15 generations (*53*). These experiments were approved by the Veterinary Office of the Canton of Bern (Switzerland; licenses BE79/11 and BE127/14). The inflammasome knockout mice for all three NLRP1 genes (*Nlrp1a/b/c*) (*54*) and NLRP3-deficient mice (*55*) on the C57BL/6 background have been previously described. Male transgenic mice in the age range of 8 to 12 weeks were compared with WT C57BL/6 mice.

Signal-modifying agents and inhibitor treatments

Inhibitors and cell signaling modification chemicals were applied to primary rat HSCs before or at the same time as FTH treatment or LPS treatments (100 ng/ml; LPS-EB from *E. coli* O111:B4, InvivoGen, #tlrl-eblps). The following inhibitors were used: NSC23766 (1 μM, no pretreatment; Cayman Chemicals, #13196), C3 transferase (1 μM, 6-hour pretreatment; Cytoskeleton Inc., #CT04), ML141 (1 μM, no pretreatment; SelleckChem, #S7686), PitStop2 (7.5 μM, no pretreatment; Abcam, #ab120687), Dyngo4a (5.7 μM, no pretreatment; Abcam, #ab120689), MCD (0.1%, no pretreatment; Sigma-Aldrich, #C4555), α-cyclodextrin (10 μM, 30-min pretreatment; Sigma-Aldrich, #C4680), Mito-TEMPO (30-min pretreatment; Cayman Chemicals, #16621, 10 μM), CA-074 methyl ester (5 μM, 30-min pretreatment; Cayman Chemicals, #18469), nocodazole (5 μM, no pretreatment; Sigma-Aldrich, #SML1665), ikarugamycin (4 μM, 30-min pretreatment; Sigma-Aldrich, #SML0188), and monensin (5 μM, no pretreatment; Sigma-Aldrich, #475895). Latrunculin A (1 μM, no pretreatment), bafilomycin (10 nM, no pretreatment), and chloroquine (100 μM, no pretreatment) were a kind gift from A. Yap (Institute for Molecular Bioscience at the University of Queensland). Latrunculin A was also purchased from Sigma-Aldrich (#C6628), and chloroquine was from Cayman Chemicals (#10010630).

Culture of human cell lines

The human HSC cell line LX-2 (a kind gift from S. Friedman, Mount Sinai School of Medicine, New York) (*56*) was cultured in Dulbecco's modified Eagle's medium (DMEM) with 2 mM glutamine, penicillin (100 U/ml), streptomycin (100 μg/ml), and 2% fetal calf serum (FCS). IHH (*57*) cells were cultured in Williams E media with 2 mM glutamine, penicillin (100 U/ml), streptomycin (100 μg/ml) and 10% FCS. HepG2 (RRID: CVCL_0027) and Hep3G (RRID: CVCL_Y479) cells (human hepatocellular carcinoma) were cultured in DMEM with 2 mM glutamine, penicillin (100 U/ml), streptomycin (100 μg/ml), and 10% FCS. All cells were cultured at 37°C under humidified 95% air and 5% CO_2. All cell lines tested negative for the presence of mycoplasma infection.

Ligand-receptor glycocapture

H-Ferritin was conjugated with TriCEPS (from DualSystems Biotech) reagent at 20°C. TriCEPS contains three functional groups: an *N*-hydroxysuccinimide ester for ligand conjugation (H-ferritin), a hydrazide group to capture glycosylated receptors, and a biotin tag for analysis by liquid chromatography tandem MS (LC-MS/MS). Cultured primary rat HSCs were detached from tissue culture plates and oxidized with sodium metaperiodate before incubation with TriCEPS-coupled H-ferritin (90 min, 4°C). After HSC lysis and biotin-mediated affinity purification of ligand/receptor glycopeptides, peptides of interest were subjected to LC-MS/MS with ligand datasets statistically analyzed for candidates of interest.

Precision-cut ex vivo liver slice culture

Precision-cut liver slices (ex vivo) were prepared using methods previously reported (*58*, *59*) from WT, ICAM-1–, NLRP1-, or NLRP3-deficient mice. All mice were male 8 to 12 weeks old. All precision-cut liver slices were produced with a WPI SYS-NVSLM1 Motorized Vibroslice except ICAM-1–deficient mice, for which a Leica VT1000S vibrating blade microtome with ice cooling was used. A minimum of four liver slices each from four or five individual mice were used for each treatment group. Liver slices were incubated with FTH (10 nM, 12 hours) or LPS (100 ng/ml, 12 hours) in M199 at 37°C. Slices were harvested for mRNA and protein and subsequent quantitation using reverse transcription quantitative polymerase chain reaction (RT-qPCR) and Western blot, respectively.

Quantitative real-time RT-PCR

Total RNA was extracted from cells/tissues using the RNeasy Kit (QIAGEN). One microgram of RNA was reverse-transcribed into cDNA using SensiFast (Bioline). Real-time PCR reactions were performed in a final volume of 15 μl with forward and reverse oligonucleotide primers used at a final concentration of 500 nM using Platinum SYBR Green qPCR SuperMix-UDG (Invitrogen) with the reaction profile as recommended by the manufacturer. PCR reaction efficiencies were between 0.95 and 1.10 (PCR primers used are listed in table S1). Melt curve analysis revealed the presence of a single product with a single melt signature. PCR was performed using an RG-6000 thermal cycler (Corbett Research, Australia). The mRNA quantitation was achieved using the two standard curve methods. Fluorescence measurements of the unknown samples were back-referenced to a standard curve relating concentration to fluorescence in arbitrary units. mRNAs were normalized to the expression of housekeeping gene basic transcription factor 3 and were expressed relative to untreated or control samples (presented as relative mRNA expression).

Transfection of plasmids expressing ICAM-1 and Rab FL and mutants

Three μg of pEGFP-C3 (GFP) or human ICAM-1–GFP cDNAs (a kind gift from F. Sanchez-Madrid, CNIC, Spain) were transfected into primary rat HSCs using LTX lipofectamine according to the

manufacturer's protocol. Experiments were performed the following day. All plasmids used were based on human cDNA sequences. For RFP-T-EEA1, mRFP-APPL1, FL pEGFP-C3-Rab5a, pEGFP-C-Rab7, pEGFP-C3-Rab11, and Rab mutants (pEGFP-C3myc-Rab5a Q79L, pEGFP-C2-Rab5 S34N, pEGFP-C-Rab7 T22N, pEGFP-C-Rab7 Q71L, pEGFP-C3-Rab11Q70L, and pEGFP-C3-Rab11 S25N), we followed similar transfection protocols as for ICAM-1–GFP. RFP-T-EEA1, mRFP-APPL1, and Rab FL and mutants were a kind gift from M. Zerial (Max Planck Institute of Molecular Cell Biology and Genetics, MPI-CBG, Dresden, Germany).

KD experiments

For KD of *Icam1*, *Cltc*, and *Grp78*, three different duplexes were pooled targeting rat ICAM-1 (NM_012967): SASI_Rn01_00094819; SASI_Rn01_00094824 and SASI_Rn01_00094825; rat CLTC SASI_Rn01_00041427; SASI_Rn01_00041429 and SASI_Rn01_00041428; or rat GRP78 (NM_013083): SASI_Rn01_00056633; SASI_Rn01_00056634, and SASI_Rn01_00056638. For KD of *Rab5a*, *Rab5b*, and *Rab5c*, we pooled 2 μg of each duplex of siRNA, which sequences were Rab5a sense 5′- GcAAGcAAGuccuAAu-AuudTsdT-3′, antisense 5′- AAuAUuAGGACUUGCUUGCdTsdT-3′; Rab5b sense 5′-cuucGuGuucuAGGuGcAAdTsdT-3′, antisense 5′-UUGcACCuAGAAcACGAAGdTsdT-3′; and Rab5c sense 5′-uAcucuAAccAAucGcAcudTsdT-3′, antisense 5′-AGUGCGAU UGGUuAGAGuAdTsdT-3′. For KD of rat *Nlrp1* and *Nlrp3* in rat HSCs, specific siRNA was obtained from Sigma-Aldrich, 5 nmol of each duplex pooled into a single tube, and the remaining 5 nmol of each individual siRNA was supplied in its own tube. The reference number for each siRNA is rat NLRP1 pool: SASI_Rn02_00391969, SASI_Rn02_00391970, SASI_Rn02_00391971, and SASI_Rn02_00391972 as well as rat NLRP3 pool: SASI_Rn02_00349589, SASI_Rn02_00349590, SASI_Rn02_00349591, and SASI_Rn02_00349592.

Dual transfections

siRNAs were transfected into primary rat HSCs as described above, followed by secondary transfection of cDNAs expressing *ICAM1*–GFP, GFP-*Rab5*, or control plasmids (GFP), to a total of total of 2 μg. GFP-*Rab5* was transfected using 0.5 to 2 μg balanced with GFP. HSCs were left for 24 hours to recover in complete M199 between the two transfections.

SDS-polyacrylamide gel electrophoresis and Western blotting

Whole primary rat HSC protein extracts were prepared by lysis of HSC cultures in radioimmunoprecipitation assay buffer and 1× SDS sample buffer [62.5 mM tris HCl (pH 6.8), 2% (w/v) SDS, 10% glycerol, 50 mM dithiothreitol, 0.01% (w/v) bromophenol blue]. Twenty micrograms of cell protein was subjected to SDS–polyacrylamide gel electrophoresis, followed by Western blot using specific antibodies. Reagents for Western blots [ASC (1:500; #sc-514414) and IL-1β clone H-153 (1:1000; #sc-7884) from Santa Cruz Biotechnology, p20 caspase-1 (1:1000; #AG-20B-0042-C100), NLRP3 (1:1000; #AG-20B-0014), and NLRP1 (1:1000; #AG-25B-0005) from Adipogen, phospho–NF-κB p65 (1:2000; #3033S) and β-actin (1:4000; #4970) from Cell Signaling Technology, and β-actin (1:4000; A5441) from Sigma-Aldrich) were probed in tris-buffered saline with Tween 20 (TBST) with 5% bovine serum albumin (BSA) powder or Licor blocking buffer with 0.1% Tween 20. For chemiluminescent Western blots, blots were probed with an anti-rabbit/goat/mouse secondary at 1:5000 to 10,000 in TBST 5% skim milk powder. Horseradish peroxidase localization was detected by Western Lightning Plus ECL (PerkinElmer) and visualized using x-ray film. For near-infrared detection, blots were probed with Licor near-infrared secondary antibodies for anti-rabbit/mouse at 1:20,000 in Licor blocking buffer with 0.1% Tween 20 and 0.01% SDS. Blots were scanned with a Licor Odyssey CLx system and quantitated with Image Studio Lite version 5.2.

Immunofluorescence

Primary rat HSCs were grown on glass coverslips and treated for 24 hours with vehicle [phosphate-buffered saline (PBS)], FTH (24 hours, 10 nM), or LPS (24 hours, 100 ng/ml). Cells were fixed with formalin, blocked with 0.2% BSA, and probed for 1 hour at room temperature with the following antibodies: ASC (1:100; Santa Cruz Biotechnology, sc-514414) and IL-1β (1:100; Santa Cruz Biotechnology, sc-7884; 1:100); Rab5 (1:100; #3547), EEA1 (1:100; #3288), APPL1 (1:100; #3858), and FTH (1:100; #4393) from Cell Signaling Technology; ICAM-1 (1:100; 10 μg/ml; AF583) from R&D Systems; E-cadherin (1:200; DAKO, M3612); and EEA1 (1:100; #610456) and ZO-1 (1:100; #610966) from BD. After this, slides were treated with AF594 donkey anti-mouse and AF488 donkey anti-rabbit (Invitrogen) at 1:500 for 1 hour, respectively. AF488-phalloidin (Life Technologies, #A12379) and AF488 conjugate cholera toxin subunit B (recombinant; Life Technologies, #C34775) were used according to the manufacturer's instructions. Glass coverslips were mounted in Prolong Gold (Molecular Probes) with 4′,6-diamidino-2-phenylindole. Images were taken with confocal microscope Zeiss 780NLO. Immunofluorescence images (63×/1.4 Oil DIC M27 1000 pixels by 1000 pixels) were quantified using MetaMorph Offline (7.8). The MetaMorph Linescan function (10-pixel width) was used to fully bisect cell bodies at 10 to 12 different locations and angles at random. Linescan image data were quantified, and edges were determined by the presence of fluorescence above background. Edges were determined to be 10 to 20 pixels in width, and the average edge fluorescence was divided by average non-edge cell body fluorescence to determine edge to body ratios.

Lipid raft (detergent-resistant membrane) preparation

Primary rat HSCs in 10-cm plates were washed 2× with cold PBS. To these, 300 μl of 1% Triton X-100 in MES-buffered saline (MBS) with protease and phosphatase inhibitors was added to the cells. The cells were scraped, transferred to new tubes, and incubated on ice for 30 min. Afterward, 0.5 ml of lysate mixed with 0.6 ml of 80% sucrose in MBS was placed at the bottom of a centrifuge tube and layered with 8 ml of 30% sucrose in MBS followed by 5% sucrose in MBS. The tubes were spun in a SW41 rotor for 18 hours at 38,000 rpm at 4°C, and 1-ml fractions were collected from the top layers of the tube.

Reactive oxygen species

An Amplex Red Hydrogen Peroxidase assay kit (Invitrogen) was used to determine whether FTH treatment (24 hours, 10 nM) caused intracellular toxicity in primary rat HSCs by generation of ROS. Carboxy-H2DCFDA, a fluorescence probe that detects intracellular hydrogen peroxide, was added 30 min before harvesting cells to measure ROS production in primary rat HSCs. Fluorescent cells were washed twice with PBS before being analyzed with a BD

FACSCalibur flow cytometer (BD Biosciences) using excitation and emission wavelengths of 492 and 517 nm, respectively. Approximately 10,000 events were recorded per sample, and the readout was analyzed using the FlowJo v10.06.

Quantification of IL-1β protein secretion from primary rat HSCs

An enzyme-linked immunosorbent assay (ELISA) against rat IL-1β (R&D Systems) was used to quantify the fold change of primary rat HSCs treated with FTH (24 hours, 10 nM). At the end of the treatment, conditioned medium was collected and measured using a 96-well polystyrene microplate coated with an IL-1β rat antibody according to the manufacturer's provided protocol. Results were normalized as fold change relative to FTH-treated HSCs in each experimental replicate unless stated otherwise. IL-1β concentrations were quantified from the absorbance at 450 nm measured on a microplate reader (BioTek PowerWave XS). All data were analyzed using GraphPad Software Inc. (USA).

FTH fluorescence labeling and MS

In preliminary studies, we treated primary rat HSCs (day 6, activated) with AF488-labeled human H-ferritin. To identify ferritin-binding proteins, primary rat HSCs were incubated first with a membrane-permeable (dimethyl pimelimidate dihydrochloride) and then a membrane-impermeable cross-linker (bis[sulfosuccinimidyl]suberate) for 30 min each at 37°C versus 4°C. Cells were lysed and spun, and membrane fraction proteins were separated by electrophoresis, with gels scanned for AF488 fluorescence. Major fluorescently labeled ferritin–cross-linked protein bands were excised and subjected to tryptic digest and identification by nano–HPLC MS/MS.

Statistical analysis

Statistical analyses were performed with GraphPad Prism version 9 (GraphPad Software Inc.). Where material is from the same mouse or same cell preparation, the analysis was performed using paired statistical tests: repeated measures one-way ANOVA with Šídák's multiple comparisons test or paired Student's *t* test, where applicable. Where material was from similar mouse groups, unpaired statistical tests were used: one-way analysis of variance (ANOVA) with Šídák's multiple comparison post hoc test or the unpaired Student's *t* test, where applicable. All statistical analysis was performed before application of fold change normalization as displayed in figures. For all qPCR and ELISA data, statistical analysis was performed on log-transformed relative expression or quantification data to create normally distributed data. Normal distribution was evaluated by QQ plots. Results are presented as mean (fold change) ± SEM. $*P \leq 0.05$, $**P \leq 0.01$, $***P \leq 0.001$, and $****P \leq 0.0001$ were used as statistical measures.

Supplementary Materials

This PDF file includes:
Figs. S1 to S9
Table S1

Other Supplementary Material for this manuscript includes the following:
MDAR Reproducibility Checklist

REFERENCES AND NOTES

1. T. Ganz, E. Nemeth, Hepcidin and disorders of iron metabolism. *Annu. Rev. Med.* **62**, 347–360 (2011).
2. M. W. Hentze, M. U. Muckenthaler, B. Galy, C. Camaschella, Two to tango: Regulation of Mammalian iron metabolism. *Cell* **142**, 24–38 (2010).
3. M. J. Wood, D. H. Crawford, L. F. Wockner, L. W. Powell, G. A. Ramm, Serum ferritin concentration predicts hepatic fibrosis better than hepatic iron concentration in human HFE-Haemochromatosis. *Liver Int.* **37**, 1382–1388 (2017).
4. K. Jurczyk, M. Wawrzynowicz-Syczewska, A. Boron-Kaczmarska, Z. Sych, Serum iron parameters in patients with alcoholic and chronic cirrhosis and hepatitis. *Med. Sci. Monit.* **7**, 962–965 (2001).
5. M. Yoneda, Y. Nozaki, H. Endo, H. Mawatari, H. Iida, K. Fujita, K. Yoneda, H. Takahashi, H. Kirikoshi, M. Inamori, N. Kobayashi, K. Kubota, S. Saito, S. Maeyama, K. Hotta, A. Nakajima, Serum ferritin is a clinical biomarker in Japanese patients with nonalcoholic steatohepatitis (NASH) independent of HFE gene mutation. *Dig. Dis. Sci.* **55**, 808–814 (2010).
6. K. Kotoh, Ueda, Tanaka, Miyazaki, K. Katou, Kohjima, M. Nakamuta, R. Takayanagi, A high prevalence of extreme hyperferritinemia in acute hepatitis patients. *Hepat. Med.* **1**, 1–8 (2009).
7. R. G. Ruddell, D. Hoang-le, J. M. Barwood, P. S. Rutherford, T. J. Piva, D. J. Watters, P. Santambrogio, P. Arosio, G. A. Ramm, Ferritin functions as a proinflammatory cytokine via iron-independent protein kinase C zeta/nuclear factor kappaB-regulated signaling in rat hepatic stellate cells. *Hepatology* **49**, 887–900 (2009).
8. F. Martinon, K. Burns, J. Tschopp, The Inflammasome. *Mol. Cell* **10**, 417–426 (2002).
9. D. Sharma, T. D. Kanneganti, The cell biology of inflammasomes: Mechanisms of inflammasome activation and regulation. *J. Cell Biol.* **213**, 617–629 (2016).
10. E. K. Jo, J. K. Kim, D. M. Shin, C. Sasakawa, Molecular mechanisms regulating NLRP3 inflammasome activation. *Cell. Mol. Immunol.* **13**, 148–159 (2016).
11. B. Todorich, X. Zhang, B. Slagle-Webb, W. E. Seaman, J. R. Connor, Tim-2 is the receptor for H-ferritin on oligodendrocytes. *J. Neurochem.* **107**, 1495–1505 (2008).
12. T. T. Chen, L. Li, D. H. Chung, C. D. C. Allen, S. V. Torti, F. M. Torti, J. G. Cyster, C. Y. Chen, F. M. Brodsky, E. C. Niemi, M. C. Nakamura, W. E. Seaman, M. R. Daws, TIM-2 is expressed on B cells and in liver and kidney and is a receptor for H-ferritin endocytosis. *J. Exp. Med.* **202**, 955–965 (2005).
13. L. Li, C. J. Fang, J. C. Ryan, E. C. Niemi, J. A. Lebrón, P. J. Björkman, H. Arase, F. M. Torti, S. V. Torti, M. C. Nakamura, W. E. Seaman, Binding and uptake of H-ferritin are mediated by human transferrin receptor-1. *Proc. Natl. Acad. Sci. U.S.A.* **107**, 3505–3510 (2010).
14. S. Geninatti Crich, M. Cadenazzi, S. Lanzardo, L. Conti, R. Ruiu, D. Alberti, F. Cavallo, J. C. Cutrin, S. Aime, Targeting ferritin receptors for the selective delivery of imaging and therapeutic agents to breast cancer cells. *Nanoscale* **7**, 6527–6533 (2015).
15. J. Y. Li, N. Paragas, R. M. Ned, A. Qiu, M. Viltard, T. Leete, I. R. Drexler, X. Chen, S. Sanna-Cherchi, F. Mohammed, D. Williams, C. S. Lin, K. M. Schmidt-Ott, N. C. Andrews, J. Barasch, Scara5 is a ferritin receptor mediating non-transferrin iron delivery. *Dev. Cell* **16**, 35–46 (2009).
16. L. Mendes-Jorge, D. Ramos, A. Valença, M. López-Luppo, V. M. R. Pires, J. Catita, V. Nacher, M. Navarro, A. Carretero, A. Rodriguez-Baeza, J. Ruberte, L-ferritin binding to scara5: A new iron traffic pathway potentially implicated in retinopathy. *PLOS ONE* **9**, e106974 (2014).
17. S. Sakamoto, H. Kawabata, T. Masuda, T. Uchiyama, C. Mizumoto, K. Ohmori, H. P. Koeffler, N. Kadowaki, A. Takaori-Kondo, H-Ferritin Is Preferentially Incorporated by Human Erythroid Cells through Transferrin Receptor 1 in a Threshold-Dependent Manner. *PLOS ONE* **10**, e0139915 (2015).
18. G. A. Ramm, R. S. Britton, R. O'Neill, B. R. Bacon, Identification and characterization of a receptor for tissue ferritin on activated rat lipocytes. *J. Clin. Invest.* **94**, 9–15 (1994).
19. C. M. Wang, S. J. Li, C. H. Wu, C. M. Hu, H. W. Cheng, J. S. Chang, Transient knock down of Grp78 reveals roles in serum ferritin mediated pro-inflammatory cytokine secretion in rat primary activated hepatic stellate cells. *Asian Pac. J. Cancer Prev.* **15**, 605–610 (2014).
20. S. V. Torti, F. M. Torti, Human H-kininogen is a ferritin-binding protein. *J. Biol. Chem.* **273**, 13630–13635 (1998).
21. N. Sheng, M. B. Fairbanks, R. L. Heinrikson, G. Canziani, I. M. Chaiken, D. M. Mosser, H. Zhang, R. W. Colman, Cleaved high molecular weight kininogen binds directly to the integrin CD11b/CD18 (Mac-1) and blocks adhesion to fibrinogen and ICAM-1. *Blood* **95**, 3788–3795 (2000).
22. L. Dewyse, H. Reynaert, L. A. van Grunsven, Best Practices and Progress in Precision-Cut Liver Slice Cultures. *Int. J. Mol. Sci.* **22**, (2021).
23. J. Dinic, H. Biverstahl, L. Maler, I. Parmryd, Laurdan and di-4-ANEPPDHQ do not respond to membrane-inserted peptides and are good probes for lipid packing. *Biochim. Biophys. Acta* **1808**, 298–306 (2011).
24. L. Jin, A. C. Millard, J. P. Wuskell, X. Dong, D. Wu, H. A. Clark, L. M. Loew, Characterization and application of a new optical probe for membrane lipid domains. *Biophys. J.* **90**, 2563–2575 (2006).
25. R. G. Parton, M. A. del Pozo, Caveolae as plasma membrane sensors, protectors and organizers. *Nat. Rev. Mol. Cell Biol.* **14**, 98–112 (2013).

26. D. E. Shvartsman, O. Gutman, A. Tietz, Y. I. Henis, Cyclodextrins but not compactin inhibit the lateral diffusion of membrane proteins independent of cholesterol. *Traffic* **7**, 917–926 (2006).
27. E. Barbieri, P. P. Di Fiore, S. Sigismund, Endocytic control of signaling at the plasma membrane. *Curr. Opin. Cell Biol.* **39**, 21–27 (2016).
28. R. Villasenor, H. Nonaka, P. Del Conte-Zerial, Y. Kalaidzidis, M. Zerial, Regulation of EGFR signal transduction by analogue-to-digital conversion in endosomes. *eLife* **4**, e06156 (2015).
29. A. McCluskey, J. A. Daniel, G. Hadzic, N. Chau, E. L. Clayton, A. Mariana, A. Whiting, N. N. Gorgani, J. Lloyd, A. Quan, L. Moshkanbaryans, S. Krishnan, S. Perera, M. Chircop, L. von Kleist, A. B. McGeachie, M. T. Howes, R. G. Parton, M. Campbell, J. A. Sakoff, X. Wang, J. Y. Sun, M. J. Robertson, F. M. Deane, T. H. Nguyen, F. A. Meunier, M. A. Cousin, P. J. Robinson, Building a better dynasore: The dyngo compounds potently inhibit dynamin and endocytosis. *Traffic* **14**, 1272–1289 (2013).
30. L. von Kleist, V. Haucke, At the crossroads of chemistry and cell biology: Inhibiting membrane traffic by small molecules. *Traffic* **13**, 495–504 (2012).
31. H. Y. Chew, P. O. de Lima, J. L. Gonzalez Cruz, B. Banushi, G. Echejoh, L. Hu, S. R. Joseph, B. Lum, J. Rae, J. S. O'Donnell, L. Merida de Long, S. Okano, B. King, R. Barry, D. Moi, R. Mazzieri, R. Thomas, F. Souza-Fonseca-Guimaraes, M. Foote, A. McCluskey, P. J. Robinson, I. H. Frazer, N. A. Saunders, R. G. Parton, R. Dolcetti, K. Cuff, J. H. Martin, B. Panizza, E. Walpole, J. W. Wells, F. Simpson, Endocytosis inhibition in humans to improve responses to ADCC-mediating antibodies. *Cell* **180**, 895–914.e27 (2020).
32. S. R. Elkin, N. W. Oswald, D. K. Reed, M. Mettlen, J. B. MacMillan, S. L. Schmid, Ikarugamycin: A natural product inhibitor of clathrin-mediated endocytosis. *Traffic* **17**, 1139–1149 (2016).
33. P. Croise, C. Estay-Ahumada, S. Gasman, S. Ory, Rho GTPases, phosphoinositides, and actin: A tripartite framework for efficient vesicular trafficking. *Small GTPases* **5**, e29469 (2014).
34. C. J. Merrifield, M. Kaksonen, Endocytic accessory factors and regulation of clathrin-mediated endocytosis. *Cold Spring Harb. Perspect. Biol.* **6**, a016733 (2014).
35. R. Villasenor, Y. Kalaidzidis, M. Zerial, Signal processing by the endosomal system. *Curr. Opin. Cell Biol.* **39**, 53–60 (2016).
36. A. Zeigerer, J. Gilleron, R. L. Bogorad, G. Marsico, H. Nonaka, S. Seifert, H. Epstein-Barash, S. Kuchimanchi, C. G. Peng, V. M. Ruda, P. D. Conte-Zerial, J. G. Hengstler, Y. Kalaidzidis, V. Koteliansky, M. Zerial, Rab5 is necessary for the biogenesis of the endolysosomal system in vivo. *Nature* **485**, 465–470 (2012).
37. S. M. Man, T. D. Kanneganti, Converging roles of caspases in inflammasome activation, cell death and innate immunity. *Nat. Rev. Immunol.* **16**, 7–21 (2016).
38. C. M. Cruz, A. Rinna, H. J. Forman, A. L. M. Ventura, P. M. Persechini, D. M. Ojcius, ATP activates a reactive oxygen species-dependent oxidative stress response and secretion of proinflammatory cytokines in macrophages. *J. Biol. Chem.* **282**, 2871–2879 (2007).
39. G. S. Lee, N. Subramanian, A. I. Kim, I. Aksentijevich, R. Goldbach-Mansky, D. B. Sacks, R. N. Germain, D. L. Kastner, J. J. Chae, The calcium-sensing receptor regulates the NLRP3 inflammasome through Ca2+ and cAMP. *Nature* **492**, 123–127 (2012).
40. R. Zhou, A. S. Yazdi, P. Menu, J. Tschopp, A role for mitochondria in NLRP3 inflammasome activation. *Nature* **469**, 221–225 (2011).
41. R. S. Britton, G. A. Ramm, J. Olynyk, R. Singh, R. O'Neill, B. R. Bacon, Pathophysiology of iron toxicity. *Adv. Exp. Med. Biol.* **356**, 239–253 (1994).
42. M. A. Krenn, M. Schürz, B. Teufl, K. Uchida, P. M. Eckl, N. Bresgen, Ferritin-stimulated lipid peroxidation, lysosomal leak, and macroautophagy promote lysosomal "metastability" in primary hepatocytes determining in vitro cell survival. *Free Radic. Biol. Med.* **80**, 48–58 (2015).
43. P. Marcellin, B. K. Kutala, Liver diseases: A major, neglected global public health problem requiring urgent actions and large-scale screening. *Liver Int.* **38**, 2–6 (2018).
44. Global Burden of Disease Cancer Collaboration, C. Fitzmaurice, T. F. Akinyemiju, F. H. Al Lami, T. Alam, R. Alizadeh-Navaei, C. Allen, U. Alsharif, N. Alvis-Guzman, E. Amini, B. O. Anderson, O. Aremu, A. Artaman, S. W. Asgedom, R. Assadi, T. M. Atey, L. Avila-Burgos, A. Awasthi, H. O. B. Saleem, A. Barac, J. R. Bennett, I. M. Bensenor, N. Bhakta, H. Brenner, L. Cahuana-Hurtado, C. A. Castañeda-Orjuela, F. Catalá-López, J.-Y. J. Choi, D. J. Christopher, S.-C. Chung, M. P. Curado, L. Dandona, R. Dandona, J. das Neves, S. Dey, S. D. Dharmaratne, D. T. Doku, T. R. Driscoll, M. Dubey, H. Ebrahimi, D. Edessa, Z. El-Khatib, A. Y. Endries, F. Fischer, L. M. Force, K. J. Foreman, S. W. Gebrehiwot, S. V. Gopalani, G. Grosso, R. Gupta, B. Gyawali, R. R. Hamadeh, S. Hamidi, J. Harvey, H. Y. Hassen, R. J. Hay, S. I. Hay, B. Heibati, M. K. Hiluf, N. Horita, H. D. Hosgood, O. S. Ilesanmi, K. Innos, F. Islami, M. B. Jakovljevic, S. C. Johnson, J. B. Jonas, A. Kasaeian, T. D. Kassa, Y. S. Khader, E. A. Khan, G. Khan, Y.-H. Khang, M. H. Khosravi, J. Khubchandani, J. A. Kopec, G. A. Kumar, M. Kutz, D. P. Lad, A. Lafranconi, Q. Lan, Y. Legesse, J. Leigh, S. Linn, R. Lunevicius, A. Majeed, R. Malekzadeh, D. C. Malta, L. G. Mantovani, B. J. M. Mahon, T. Meier, Y. A. Melaku, M. Melku, P. Memiah, W. Mendoza, T. J. Meretoja, H. B. Mezgebe, T. R. Miller, S. Mohammed, A. H. Mokdad, M. Moosazadeh, P. Moraga, S. M. Mousavi, V. Nangia, C. T. Nguyen, V. M. Nong, F. A. Ogbo, A. T. Olagunju, M. Pa, E.-K. Park, T. Patel, D. M. Pereira, F. Pishgar, M. J. Postma, F. Pourmalek, M. Qorbani, A. Rafay, S. Rawaf, D. L. Rawaf, G. Roshandel, S. Safiri, H. Salimzadeh, J. R. Sanabria, M. M. S. Milicevic, B. Sartorius, M. Satpathy, S. G. Sepanlou, K. A. Shackelford, M. A. Shaikh, M. Sharif-Alhoseini, J. She, M.-J. Shin, I. Shiue, M. G. Shrime, A. H. Sinke, M. Sisay, A. Sligar, M. B. Sufiyan, B. L. Sykes, R. Tabarés-Seisdedos, G. A. Tessema, R. Topor-Madry, T. T. Tran, B. X. Tran, K. N. Ukwaja, V. V. Vlassov, S. E. Vollset, E. Weiderpass, H. C. Williams, N. B. Yimer, N. Yonemoto, M. Z. Younis, C. J. L. Murray, M. Naghavi, Global, regional, and national cancer incidence, mortality, years of life lost, years lived with disability, and disability-adjusted life-years for 29 cancer groups, 1990 to 2016. *Oncologia* **4**, 1553–1568 (2018).
45. M. Worwood, Ferritin. *Blood Rev.* **4**, 259–269 (1990).
46. L. S. Feder, J. A. Todaro, D. L. Laskin, Characterization of interleukin-1 and interleukin-6 production by hepatic endothelial cells and macrophages. *J. Leukoc. Biol.* **53**, 126–132 (1993).
47. P. F. Lalor, P. Shields, A. Grant, D. H. Adams, Recruitment of lymphocytes to the human liver. *Immunol. Cell Biol.* **80**, 52–64 (2002).
48. H. Yokomori, M. Oda, M. Ogi, G. Wakabayashi, S. Kawachi, K. Yoshimura, T. Nagai, M. Kitajima, M. Nomura, T. Hibi, Expression of adhesion molecules on mature cholangiocytes in canal of Hering and bile ductules in wedge biopsy samples of primary biliary cirrhosis. *World J. Gastroenterol.* **11**, 4382–4389 (2005).
49. N. Reglero-Real, A. Álvarez-Varela, E. Cernuda-Morollón, J. Feito, B. Marcos-Ramiro, L. Fernández-Martín, M. J. Gómez-Lechón, J. Muntané, P. Sandoval, P. L. Majano, I. Correas, M. A. Alonso, J. Millán, Apicobasal polarity controls lymphocyte adhesion to hepatic epithelial cells. *Cell Rep.* **8**, 1879–1893 (2014).
50. C. Ferreira, D. Bucchini, M. E. Martin, S. Levi, P. Arosio, B. Grandchamp, C. Beaumont, Early embryonic lethality of H ferritin gene deletion in mice. *J. Biol. Chem.* **275**, 3021–3024 (2000).
51. P. Santambrogio, S. Levi, A. Cozzi, E. Rovida, A. Albertini, P. Arosio, Production and characterization of recombinant heteropolymers of human ferritin H and L chains. *J. Biol. Chem.* **268**, 12744–12748 (1993).
52. J. L. Dunne, R. G. Collins, A. L. Beaudet, C. M. Ballantyne, K. Ley, Mac-1, but not LFA-1, uses intercellular adhesion molecule-1 to mediate slow leukocyte rolling in TNF-alpha-induced inflammation. *J. Immunol.* **171**, 6105–6111 (2003).
53. G. U. Enzmann, S. Pavlidou, M. Vaas, J. Klohs, B. Engelhardt, ICAM-1(null) C57BL/6 mice are not protected from experimental ischemic stroke. *Transl. Stroke Res.* **9**, 608–621 (2018).
54. S. L. Masters, M. Gerlic, D. Metcalf, S. Preston, M. Pellegrini, J. A. O'Donnell, K. McArthur, T. M. Baldwin, S. Chevrier, C. J. Nowell, L. H. Cengia, K. J. Henley, J. E. Collinge, D. L. Kastner, L. Feigenbaum, D. J. Hilton, W. S. Alexander, B. T. Kile, B. A. Croker, NLRP1 inflammasome activation induces pyroptosis of hematopoietic progenitor cells. *Immunity* **37**, 1009–1023 (2012).
55. F. Martinon, V. Petrilli, A. Mayor, A. Tardivel, J. Tschopp, Gout-associated uric acid crystals activate the NALP3 inflammasome. *Nature* **440**, 237–241 (2006).
56. L. Xu, A. Y. Hui, E. Albanis, M. J. Arthur, S. M. O'Byrne, W. S. Blaner, P. Mukherjee, S. L. Friedman, F. J. Eng, Human hepatic stellate cell lines, LX-1 and LX-2: New tools for analysis of hepatic fibrosis. *Gut* **54**, 142–151 (2005).
57. I. J. Schippers, H. Moshage, H. Roelofsen, M. Müller, H. S. A. Heymans, M. Ruiters, F. Kuipers, Immortalized human hepatocytes as a tool for the study of hepatocytic (de-) differentiation. *Cell Biol. Toxicol.* **13**, 375–386 (1997).
58. G. N. Gobert, S. K. Nawaratna, M. Harvie, G. A. Ramm, D. P. McManus, An ex vivo model for studying hepatic schistosomiasis and the effect of released protein from dying eggs. *PLOS Negl. Trop. Dis.* **9**, e0003760 (2015).
59. M. A. Pearen, H. K. Lim, F. D. Gratte, M. A. Fernandez-Rojo, S. K. Nawaratna, G. N. Gobert, J. K. Olynyk, J. E. E. Tirnitz-Parker, G. A. Ramm, Murine precision-cut liver slices as an ex vivo model of liver biology. *J. Vis. Exp.* **157**, e60992 (2020).

Acknowledgments: We are thankful to R. Parton from University of Queensland, Brisbane, Australia for the constructive comments on this manuscript; A. Yap (Institute for Molecular Bioscience at the University of Queensland) for the gift of bafilomycin and chloroquine, M. Zerial from the Max-Planck in Dresden, Germany; and H. Quek from the QIMR Berghofer MRI for the gift of IL-1β antibody. We thank S. Forbes from the University of Edinburgh for comments and helpful suggestions to improve this manuscript. **Funding:** This work was supported by research grants from the National Health and Medical Research Council (NHMRC) of Australia (grant nos. APP1048740 to G.A.R. and APP1124026 to A.J.B. and M.A.F.-R.). M.A.F.-R. is supported by the grants from the Talento Program from the Madrid Government of Spain (grant nos. T1-BIO-1854 and 2020-5A_BIO-19724). M.P.I. was supported by the AMAROUT Marie Curie program (no. 291803-AMAROUT II) and by the TALENTO Program by the Regional Madrid Government (2018-T1/BIO-11262). G.A.R. was supported by a Research Fellowship from the NHMRC of Australia (grant no. APP1061332). **Author contributions:**

M.A.F.-R. and G.A.R. conceived, designed, performed experiments, interpreted data, and wrote the manuscript. A.G.B. and A.J. performed the FTH protein binding experiments and MS analysis. M.P.I. carried out ROS and ELISA assays. D.H.-L. and M.A.P. isolated HSCs and performed gene expression analysis. S.S.K.N. and G.N.G. developed and performed WT ex vivo mouse liver slice experiments. M.A.P., S.L.S, R.R., U.D., and B.E. assisted in the performance of the ex vivo liver slice experiments on ICAM-1, NLRP1, and NLRP3 knockout mouse livers. M.A.P., B.G., and S.L.S. performed the ICAM-1 trafficking and immunofluorescence. M.P. and P.A. synthesized the recombinant FTH protein. A.J.B. provided reagents and intellectual input. All authors have read, critically reviewed, and provided feedback on the manuscript. **Competing interests:** M.A.F.-R. and G.A.R. are the authors of a Patent Cooperation Treaty (PCT): PCT/AU2018/050427. The other authors declare that they have no competing interests. **Data and materials availability:** The MS data were deposited into the PRIDE repository (www.ebi.ac.uk/pride/) with the identifier PXD048779. All other data needed to evaluate the conclusions in the paper are present in the paper or the Supplementary Materials.

Submitted 17 August 2022
Resubmitted 26 July 2023
Accepted 11 March 2024
Published 2 April 2024
10.1126/scisignal.ade4335